

Aus dem Institut für Muskuloskelettale Medizin (IMM)
Klinikum der Ludwig-Maximilians-Universität München



Investigating the role of ADAR2 in osteoblast and adipocyte differentiation

Dissertation

zum Erwerb des Doktorgrades der Medizin

an der Medizinischen Fakultät der

Ludwig-Maximilians-Universität zu München

vorgelegt von

Rui Tang

aus

Henan, China

Jahr

2022

Mit Genehmigung der Medizinischen Fakultät der
Ludwig-Maximilians-Universität zu München

Erster Gutachter: Univ. Prof. Dr. Dr. Eric Hesse

Zweiter Gutachter: Univ. Prof. Dr. Hanna Taipaleenmäki

Dritter Gutachter: Priv. Doz. Dr. med. Elias Volkmer

ggf. weitere Gutachter:

Mitbetreuung durch die
promovierten Mitarbeiter: Univ. Prof. Dr. Hanna Taipaleenmäki, Dr. Hiroaki
Saito

Dekan: Prof. Dr. med. Thomas Gudermann

Tag der mündlichen Prüfung: 15.11.2022

Table of Content

Table of Content	3
Zusammenfassung (Deutsch):	6
Abstract (English):	8
List of figures	9
List of tables	10
List of abbreviations	11
1. Introduction	12
1.1 Bones	12
1.1.1 Bone tissue	12
1.1.2 Bone remodeling and modeling	14
1.2 Bone marrow	15
1.3 Mesenchymal stem cells (MSCs)	16
1.3.1 Osteoblast differentiation	18
1.3.2 Adipocyte differentiation	19
1.3.3 Epigenetic modifications in MSCs differentiation	22
1.4 Adenosine deaminase on double-strand RNA (ADAR)	22
1.4.1 Members of the ADAR family	23
1.4.2 Editing mechanism and selectivity	24
1.4.3 Functional implication of A-to-I editing	25
1.4.4 ADAR-related diseases	28
2. Hypothesis	30
2.1 Hypothesis	30
2.2 Aims	30
3. Material and Methods	31
3.1 Chemicals, equipment and consumables	31
3.2 Kits	34
3.3 Oligonucleotides	35
3.4 Antibodies	36
3.5 siRNA	36
3.6 Software	36
3.7 Cell culture	37
3.7.1 Cell line	37

3.7.2	Culture conditions	37
3.7.3	Cell culture splitting	37
3.7.4	Cell counting	37
3.7.5	Cell differentiation	38
3.8	Transient transfection	39
3.9	Staining methods	39
3.9.1	Alkaline phosphatase staining	39
3.9.2	Alizarin red staining	40
3.9.3	Oil red O staining	40
3.10	RNA isolation	42
3.10.1	RNeasy kit method	42
3.10.2	Trizol method	43
3.11	cDNA synthesis	43
3.12	Quantitative real-time PCR (qPCR) analysis	44
3.13	Immuno-blot analysis	45
3.13.1	Cell lysate preparation	45
3.13.2	Quantification of protein concentration	46
3.13.3	Protein gel electrophoresis	46
3.13.4	Protein transfer	47
3.13.5	Antibody incubation	48
3.13.6	Chemiluminescence imaging	48
3.14	RNA sequencing	49
3.14.1	Target specific reverse transcription	49
3.14.2	Transcript purification	50
3.14.3	Sanger sequencing	51
3.15	Statistical analysis	51
4.	Results	52
4.1	ADAR2 expression is increased during osteoblast differentiation	52
4.2	Inhibition of ADAR2 expression does not affect osteoblast differentiation ...	54
4.3	ADAR2 expression is increased during adipocyte differentiation	57
4.4	Inhibition of ADAR2 expression decreases adipocyte differentiation	59
4.5	Inhibition of ADAR2 expression impairs editing of GRIA2 during adipocyte differentiation	62
5.	Discussion	66
	References	73

Acknowledgements	87
Affidavit	88
Curriculum vitae	错误! 未定义书签。

Zusammenfassung (Deutsch):

Knochen stützen den Körper und sind an Stoffwechselprozessen beteiligt. Das Knochengewebe wird stetig umgebaut, um die Integrität zu bewahren. Der Erhalt der Knochenmasse hängt von einer ausgewogenen osteoklastären Knochenresorption sowie einer von mesenchymalen Osteoblasten-abhängigen Knochenbildung ab. Mesenchymale Stammzellen (MSCs) sind Vorläuferzellen im Knochenmark, die die Knochenmasse beeinflussen können, indem sie sich zu Osteoblasten oder Adipozyten differenzieren. Die Mechanismen, die an der Differenzierung in beide Linien beteiligt sind, sind noch nicht vollständig aufgeklärt. Aus wissenschaftlicher und translationaler Sicht ist es jedoch sehr wichtig, mehr Einblicke in diesen Prozess zu erhalten. Eine in unserem Labor durchgeführte Sequenzanalyse ergab, dass das Gen *adenosine deaminase on double-strand RNA 2* (ADAR2) in Knochenproben von Patienten mit geringer Knochenmasse stark exprimiert wurde. Als post-transkriptioneller RNA-Editor vermittelt ADAR2 Nukleotidumwandlungen, die sich auf die RNA-Biogenese, RNA-Interferenz, Proteinerzeugung und -funktion auswirken können. Unter Verwendung von immortalisierten MSCs (hMSC-TERTs) zeigt diese Arbeit auf, dass die Expression von ADAR2 während der Differenzierung zu Osteoblasten und Adipozyten zunahm. Weitere Untersuchungen zeigten, dass die vorübergehende Hemmung von ADAR2 die Differenzierung von Osteoblasten nicht betraf, aber die von Adipozyten stark beeinträchtigte, ohne die Expression des Master-Transkriptionsfaktors PPAR γ zu beeinflussen. Eine Sanger-Sequenzierung ergab ein reduziertes ADAR2-abhängiges *A-to-I editing* an der Q/R-Stelle der *Glutamate Ionotropic Receptor AMPA Type Subunit 2* (GRIA2). Dies hemmt die Umwandlung des AMPA-Rezeptors von Ca²⁺-durchlässig zu undurchlässig. Vermutlich übt die erhöhte intrazelluläre Ca²⁺-Konzentration einen negativen Einfluss auf die Transkriptionsaktivität von PPAR γ und die Adipozytendifferenzierung aus. Zusammenfassend zeigt diese Arbeit eine neue ADAR2-vermittelte epigenetische Modifikation, die die Adipozyten-Differenzierung von MSCs unterstützt. Mechanistisch ermöglicht ADAR2 das *A-to-I editing* der GRIA2-Q/R-Stelle, was vermutlich zu einem reduzierten Ca²⁺-Einstrom führt und die Adipogenese fördert, indem sie die Transkriptionsaktivität von PPAR γ erhält. Diese Erkenntnisse sind neuartig, original und tragen zum Verständnis der MSC-Differenzierung in

Adipozyten bei. Darüber hinaus sind die Ergebnisse im Kontext von Erkrankungen mit geringer Knochenmasse von translationalem Wert.

Abstract (English):

Bones provide mechanical support to the body and are involved in various metabolic processes. Bone tissue is constantly remodeled throughout life to preserve integrity and functionality. Maintenance of bone mass depends on a balanced bone resorption mediated by osteoclasts and mesenchyme-derived osteoblast-dependent bone formation. Mesenchymal stem cells (MSCs) are multipotent precursor cells located in the bone marrow that can affect bone mass by differentiating either into osteoblasts or adipocytes. Although the field has made great advances during the last two decades, the mechanisms involved in the differentiation into either lineage are not yet fully elucidated. However, obtaining more insights into this process is very important from a scientific and translational point. A sequencing analysis conducted in our laboratory revealed that the gene of adenosine deaminase on double-strand RNA 2 (ADAR2) was highly expressed in bone samples obtained from patients with relatively lower bone mass. As post-transcriptional RNA editor, ADAR2 mediates nucleotide conversion that may impact RNA biogenesis, RNA interference, protein generation and function. Using immortalized MSCs (hMSC-TERTs), this thesis uncovered that expression of ADAR2 increased during MSC differentiation towards osteoblasts and adipocytes. Further investigations demonstrated that transient inhibition of ADAR2 did not affect osteoblast differentiation but greatly impaired adipocyte differentiation without altering the expression of the master transcription factor PPAR γ . Sanger sequencing revealed a reduced ADAR2-dependent A-to-I editing at the Q/R site of the Glutamate Ionotropic Receptor AMPA Type Subunit 2 (GRIA2). Impaired editing of the GRIA2 Q/R site inhibits the conversion of the AMPA receptor from Ca²⁺ permeable to impermeable. Presumably, the elevated intracellular Ca²⁺ concentration exerts a negative impact on PPAR γ transcriptional activity and adipocyte differentiation. In summary, this study unraveled a novel epigenetic modification mediated by ADAR2 supporting adipocyte differentiation of MSCs. Mechanistically, ADAR2 facilitates A-to-I editing of the GRIA2 Q/R site, leading to a reduced Ca²⁺ influx. The reduced Ca²⁺ permeability promotes adipogenesis by preserving PPAR γ transcriptional activity. These findings are novel, original and contribute to the understanding of MSC differentiation into adipocytes. Furthermore, the results are of translational value given a potential implication in low bone mass diseases in humans.

List of figures

Figure 1.1. Schematic of the bone structure.	
Figure 1.2. Schematic of bone remodeling.	
Figure 1.3. Bone marrow conversion from newborn to adult period.	
Figure 1.4. Multi-potential differentiation capacity of MSCs.....	
Figure 1.5. Osteoblast differentiation.	
Figure 1.6. Transcriptional regulation of adipocyte differentiation.	
Figure 1.7. Schematic of ADAR-mediated adenosine deamination.	
Figure 1.8. Structure of ADAR family members.	
Figure 1.9. mRNA processing.	
Figure 1.10. ADAR2-mediated editing of GRIA2.	
Figure 1.11. A-to-I editing on non-coding regions of mRNA.	
Figure 3.1. Work flow to obtain larger images of Oil red O-stained cell layers.	
Figure 4.1. hMSC-TERTs differentiate into osteoblasts.	
Figure 4.2. ADAR2 mRNA expression is increased during osteoblast differentiation.	
Figure 4.3. Transient siRNA transfection decreases ADAR2 expression without affecting ADAR1 expression during osteoblast differentiation.	
Figure 4.4. Inhibition of ADAR2 expression does not affect osteoblast differentiation.	
Figure 4.5. hMSC-TERTs differentiate into adipocytes.	
Figure 4.6. ADAR2 mRNA expression increases during adipocyte differentiation.	
Figure 4.7. Inhibition of ADAR2 expression does not affect abundance of ADAR1 mRNA during adipocyte differentiation.	
Figure 4.8. Inhibition of ADAR2 expression impairs late-stage adipocyte differentiation.	
Figure 4.9. Inhibition of endogenous ADAR2 mRNA expression attenuates late-stage adipocyte differentiation.	
Figure 4.10. Obtaining transcripts of the GRIA2 Q/R site.	
Figure 4.11. Inhibition of ADAR2 impairs A-to-I editing of the Q/R site of the GRIA2 mRNA.	

List of tables

Table 3.1. List of chemicals used

Table 3.2. List of equipment used.....

Table 3.3. List of consumables used

Table 3.4. List of kits used

Table 3.5. List of oligonucleotides used

Table 3.6. List of antibodies used

Table 3.7. List of siRNA used

Table 3.8. List of software used

List of abbreviations

Activating transcription factor 4	ATF4
Adenosine deaminase on double-strand RNA	ADAR
Adiponectin	ADIPOQ
Aicardi–Goutières syndrome	AGS
Alkaline phosphatase	ALP
Bone morphogenetic protein	BMP
CAAT/enhancer-binding protein	C/EBP
cAMP response element-binding protein	CREB
Collagen type 1 alpha 1	COL1A1
Dyschromatosis symmetrica hereditaria	DSH
Fatty acid-binding protein	FABP
Fibroblast growth factor	FGF
Glutamate ionotropic receptor AMPA type subunit	GRIA
Glyceraldehyde 3-phosphate dehydrogenase	GAPDH
Hedgehog	HH
Hematopoiesis stem cell	HSC
Insulin-like growth factor	IGF
Mesenchymal stem cell	MSC
Osteocalcin	OCN
Parathyroid hormone	PTH
Proliferator-activated receptor γ	PPAR γ
Quantitative real-time PCR	qPCR
Runt-related transcription factor 2	RUNX2
Telomerase reverse transcriptase	TERT
Transforming growth factor	TGF
Tumor necrosis factor	TNF
Untranslated region	UTR
α -amino-3-hydroxy-5-methyl-4-isoxazolepropionic acid receptor	AMPA

1. Introduction

Health and integrity of bones are essential for vertebrates. In adults, maintenance of bone mass requires a balanced bone formation and bone resorption¹. Mesenchymal stem cells (MSCs) are multipotent stromal cells located in the bone marrow that can differentiate into osteoblasts and adipocytes². Osteoblasts are bone-forming cells that generate bone matrix and facilitate matrix mineralization³. Adipocytes are the main energy-storing cells containing abundant lipid droplets⁴. Differentiation of MSCs is tightly regulated, which influences bone formation and bone resorption. Discovering the regulation of MSCs differentiation increases the understanding of bone biology and might benefit the treatment of diseases with abnormal bone mass like osteoporosis.

1.1 Bones

An adult human skeleton comprises 213 bones with some variability between individuals¹. According to their shapes, bones are classified into 4 groups: 1) Long bones (e.g. femur, tibia) are located in limbs comprising a thin tubular diaphysis flanked by two inflated metaphyses at both ends. 2) Short bones (e.g. carpal and tarsal bones) are shaped square and can be found in joints like wrists and ankles. 3) Flat bones (e.g. skull, ribs) are characterized by a large surface. 4) Irregular bones (e.g. vertebrae, sacrum) have special appearances and can provide various and complex functions¹. In addition, there is a group of small bones with variable numbers named sesamoid bones, which are embedded in muscles or tendons. The patella is the largest sesamoid bone providing stability and function to the knee joint⁵.

Bones constitute the structural body frame of vertebrates. Mechanically, bones provide physical support, protect inner organs, and allow locomotion by interacting with muscles and ligaments. In addition, bones serve as mineral storage and provide endocrine functions^{1,6}.

1.1.1 Bone tissue

Bone is a rigid connective tissue rich in collagen matrix and mineralized with inorganic salt (mainly calcium phosphate)⁷. Except for articular joint surfaces, all bones are covered with a dense fibrous membrane called periosteum, and a thin

membrane named endosteum that lines the inner surface. The periosteum contains nerves and vessels, which contribute to pain sensation and blood supply⁸.

Bone tissue is separated into cortical bone (also called compact bone) and trabecular bone (also called spongy or cancellous bone). Cortical bone forms the solid outer shell of bones, which accounts for about 80% of the total bone mass. The basic functional unit of cortical bone is the osteon (also called Haversian system). Osteons are oriented alongside the axis of bones and are of cylindrical shape. The microstructure of an osteon comprises a Haversian canal in the center, which is surrounded by multiple concentric layers of lamellar bone (aligned collagen fibers). Small blood vessels and nerve fibers travel through the canal. At the vertical axis, transport vessels (also called Volkmann tubes or perforating canals) traverse the bones and connect osteons with each other and with the periosteum (Fig. 1.1)⁹. Trabecular bone is located inside the bones, in long bones primarily in the metaphysis, and accounts for the remaining 20% of the bone mass. Trabecular bone is less dense than cortical bone and consists of interconnected trabeculae that are oriented in the direction of mechanical loading to bear the weight and forces (Fig. 1.1)¹⁰.

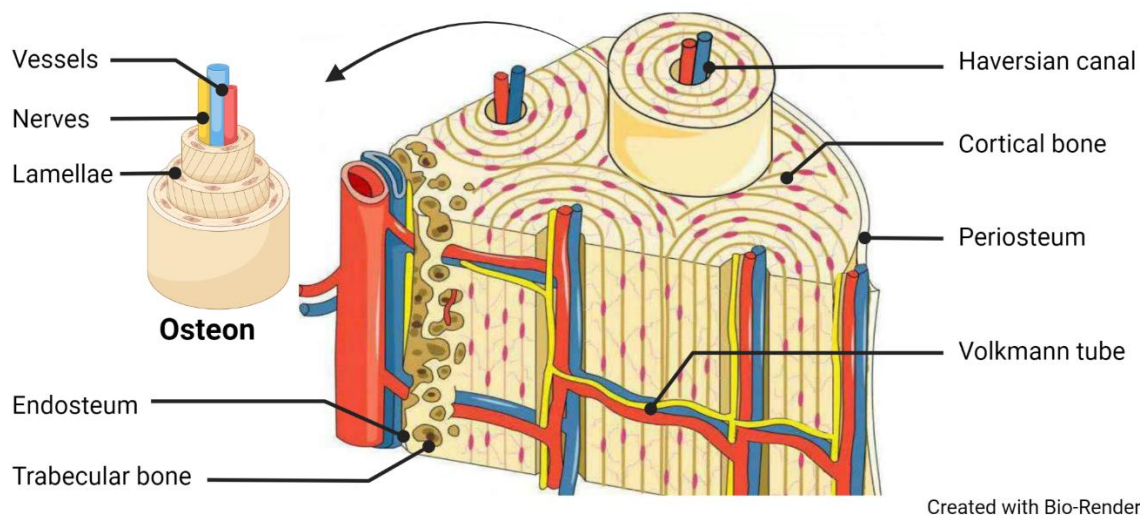


Figure 1.1. Schematic of the bone structure. Bone tissue comprises the dense outer cortical bone and the less dense inner trabecular bone. The basic functional unit of cortical bone is the osteon. Each osteon contains a Haversian canal in the center, which is surrounded by bone lamellae and contains nerves and vessels. Volkmann tubes connect vessels and nerve fibers in Haversian canals with periosteum and endosteum.

1.1.2 Bone remodeling and modeling

Bone tissue is dynamic and undergoes constant osteoclast-mediated resorption and osteoblast-dependent formation throughout life¹¹. Bone remodeling occurs on surfaces triggered by local injuries like micro-cracks. This damage results in the accumulation of monocyte-macrophage lineage cells, which are precursor cells of osteoclasts. To mediate bone resorption, mature osteoclasts form an actin ring and adhere to the bone surface with their ruffled border and absorb bone matrix by generating acids and enzymes¹². After resorption, mesenchymal lineage-derived osteoblast precursor cells migrate into the resorption area and begin to differentiate into mature osteoblasts. Mature osteoblasts have a cuboidal shape and are localized on bone surfaces. To generate new bone tissue, mature osteoblasts secrete large amounts of not yet mineralized organic substrate rich in collagen type 1 alpha 1 (COL1A1) and osteoid¹³. In addition, alkaline phosphatase (ALP) is also secreted into the matrix and supports the mineralization into hydroxyapatite¹⁴. Upon matrix production, osteoblasts become quiescent on bone surfaces as lining cells, get embedded into the mineralizing matrix as osteocytes, or undergo apoptosis (Fig 1.2)³. Balanced bone remodeling contributes to maintaining bone mass and quality.

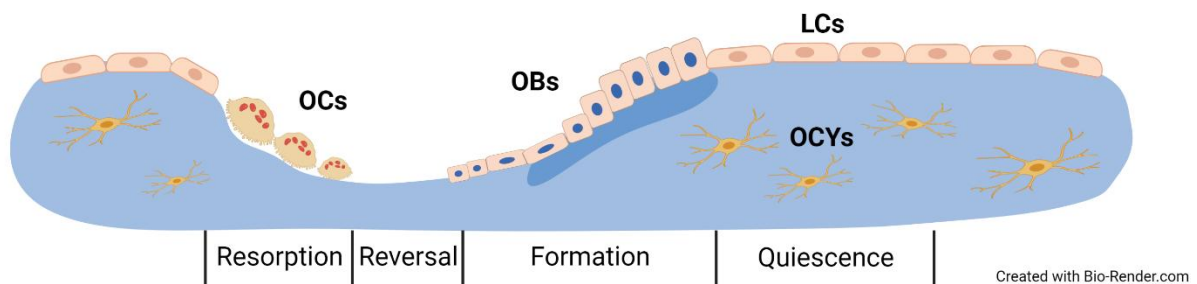


Figure 1.2. Schematic of bone remodeling. Bone remodeling starts with osteoclast (OC)-dependent bone resorption. After reversal, osteoblast (OB)-mediated bone formation begins. Following mineralization, osteoblasts become quiescent on bone surfaces as lining cells (LCs), are embedded into the mineralized matrix as osteocytes (OCYs), or undergo apoptosis (not shown).

Different from remodeling, bone modeling is a process of bone formation that occurs on quiescent surfaces without prior bone resorption and therefore in an uncoupled manner. Bone remodeling and modeling both occur during the development and

growth stages, with modeling being dominant. After adulthood, modeling and remodeling continue but remodeling becomes dominant¹¹.

1.2 Bone marrow

Comprising around 5% of total body weight, bone marrow is a type of semi-solid tissue, which resides in the medullary cavity of long bones and empty spaces of trabecular bones (like ribs, vertebrae, and pelvis)¹⁵.

Bone marrow is the main site of postnatal hematopoiesis containing different types and differentiation stages of blood cells. Hematopoietic stem cells (HSCs) as the common progenitors of both myeloid and lymphoid lineage cells are located in the bone marrow. Proliferation and maturation of HSCs are all partly or completely achieved within the bone marrow¹⁶. In addition, bone marrow contains or is in close contact with non-hematopoietic cells such as adipocytes, osteoblasts, osteoclasts, endothelial cells, and nerve cells, which contribute to the micro-environment for hematopoiesis¹⁷.

Bone marrow is heterogeneous and distributions of hematopoietic cells and of non-hematopoietic cells may vary. According to the color, bone marrow can be separated into two types: red- and yellow bone marrow¹⁸. Red bone marrow has intensive hematopoietic activity containing massive blood cells supported by reticular cells and adipocytes. Red bone marrow comprises approximately 40% water, 40% fat, and 20% protein¹⁸. Yellow bone marrow indicates marrow tissue with less hematopoietic activity, which mostly consists of adipocytes. Since fat tissue constitutes 80% of yellow bone marrow, it is also named bone marrow fat¹⁹.

Components of red and yellow bone marrow change with aging. In infants, bone marrow is completely red. Then, red bone marrow is gradually replaced by yellow bone marrow. In adulthood, red bone marrow is only rarely scattered in metaphyses (Fig 1.3)²⁰. This conversion from red to yellow bone marrow also happens under pathological conditions like obesity, type 2 diabetes, and osteoporosis¹⁸. Reversed conversion is observed in smoking patients, which is likely caused by hypoxia-induced increasing demanding of hematopoiesis²¹.

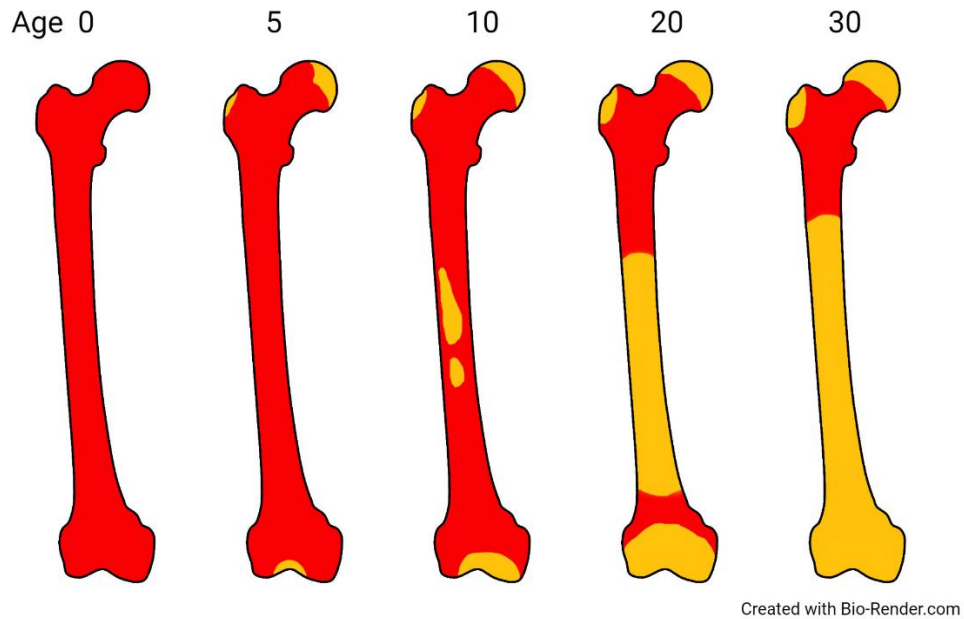


Figure 1.3. Bone marrow conversion from newborn to adult. In infants, bone marrow is completely red and full of hematopoietic tissue. At the age of 5, yellow bone marrow emerges in metaphyses. In the teenager period, red to yellow conversion begins in the center of the diaphysis and expands. Until 30 years old, red bone marrow only scatters in the proximal metaphysis.

1.3 Mesenchymal stem cells (MSCs)

Bone marrow also contains a type of non-hematopoietic stromal cells that retain a self-renewal and multipotent capacity. In the 1970s, Alexander Friedenstein first isolated a group of colony forming fibroblast-like cells from bone marrow, which can proliferate and differentiate into osteoblasts, adipocytes, and chondroblasts *in vitro*²²⁻²⁴. Due to the ability of these cells to differentiate into connective tissue cells, Caplan suggested to name these cells as mesenchymal stem cells (MSCs)²⁵. In 2006, the International Society for Cellular Therapy (ISCT) proposed the minimal criteria for human MSCs: 1) MSCs must be plastic-adherent in standard culture conditions. 2) MSCs must present surface markers including CD105, CD73, and CD90, but do not express CD45, CD34, CD14 or CD11b, CD79a or CD19, and HLA-DR. 3) MSCs must have the ability to differentiate into osteoblasts, adipocytes, and chondroblasts²⁶.

The frequency of MSCs is very low with less than 0.1% of all cells in bone marrow²⁷. Beyond bone marrow, MSCs have also been reported to be isolated from other organs including adipose tissue²⁸, peripheral blood²⁹, dental pulps³⁰, endometrium³¹, and fetal tissues³²⁻³⁴. However, MSCs derived from different organs have different features. For example, MSCs originating from fetal tissues have a

higher proliferation ability compared with MSCs derived from the bone marrow³⁵. MSCs derived from bone marrow have higher stemness since they form more colonies *in vitro*³⁶. MSCs may also behave differently between individuals. Phinney et al. observed bone marrow-derived MSCs from 17 healthy adults of different ages. They reported that abilities of proliferation and osteogenesis are around 10 times variation among all samples³⁷. Moreover, another study concluded this difference is age-related: MSCs proliferation and osteoblast differentiation decrease with age while apoptosis increases conversely³⁸.

MSCs have a strong differentiation ability. The traditional dogma postulates that MSCs are mesoderm-derived and can only differentiate into connective tissue cells like osteoblasts, adipocytes, and chondroblasts. However, recent studies reported that under certain conditions, MSCs can also differentiate into endoderm and ectoderm lineage cells like hepatocytes, β -cells of pancreatic islets^{39,40}, and nerve cells⁴¹.

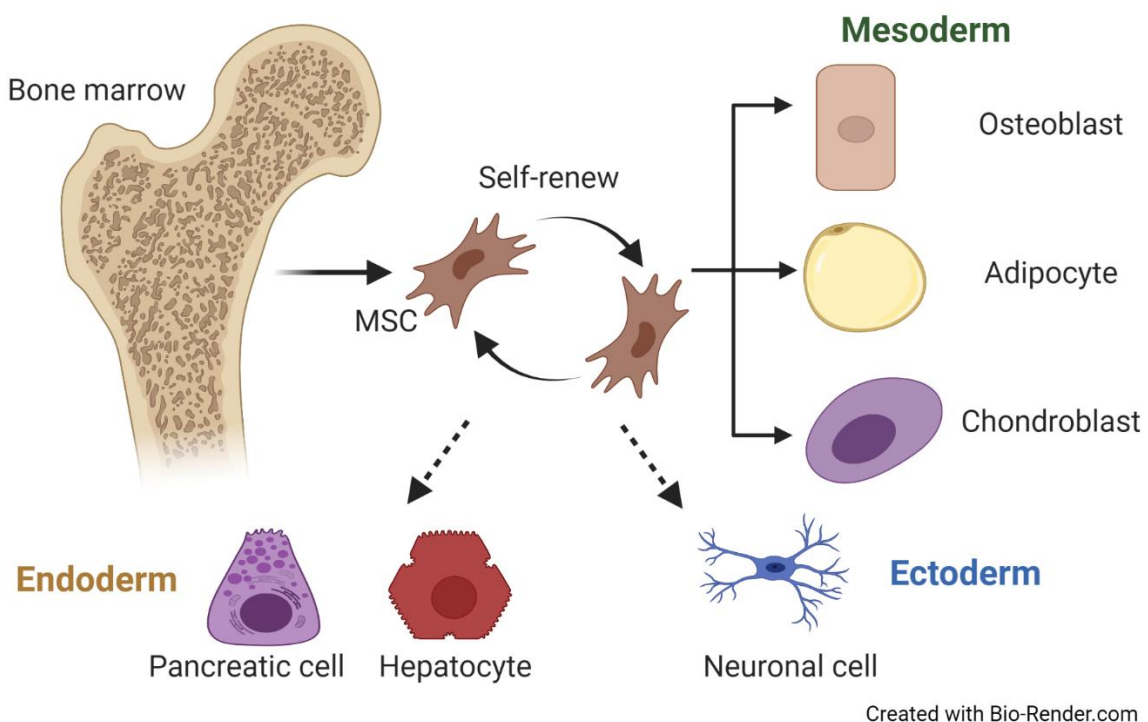
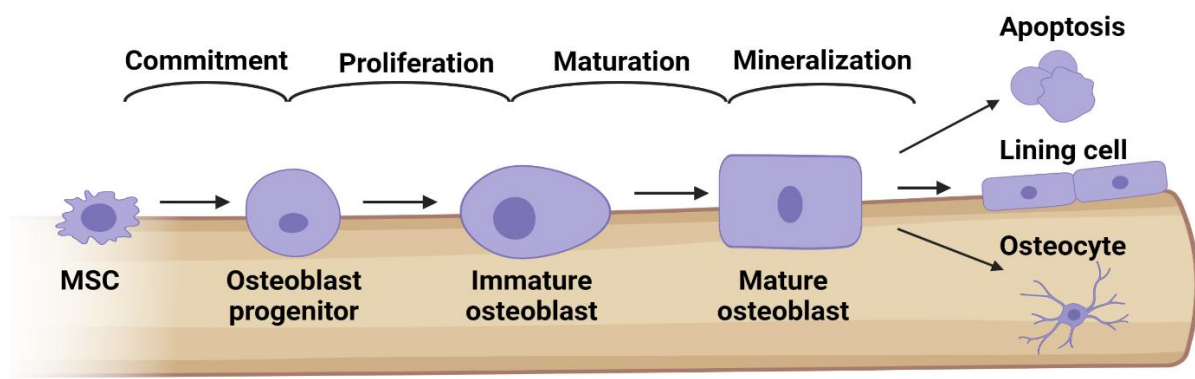


Figure 1.4. Multi-potential differentiation capacity of MSCs. Bone marrow-derived MSCs have the ability to self-renew (curved arrow) and can differentiate into osteoblasts, adipocytes, and chondroblasts (straight, solid arrows). Under special circumstances, MSCs can also differentiate into ectodermal or endodermal lineage cells *in vitro* (dashed arrows).

MSCs have great potential for clinical treatment concepts, especially in tissue repair⁴². Besides replacing injured cells by differentiation, MSCs secrete paracrine factors including extracellular matrix enzymes, binding proteins, growth factors, and hormones to facilitate tissue repair⁴³. Moreover, MSCs generate cytokines like interferons, tumor necrosis factors (TNFs), and interleukins to modulate immune reactions⁴⁴.

1.3.1 Osteoblast differentiation

Osteoblasts are cuboidal-shaped bone-forming cells that originate from MSCs. After commitment, osteoblast progenitor cells proliferate and differentiate into mature osteoblasts, which lay down a new bone matrix (osteoid) that mineralizes later (Fig. 1.5)^{45,46}.



Created with Bio-Render.com

Figure 1.5. Osteoblast differentiation. Arising from MSCs, osteoblast progenitor cells differentiate into mature osteoblasts through 3 stages: proliferation, matrix maturation, and mineralization. After that, osteoblasts either become entrapped in the mineralized matrix as osteocytes, rest on quiescent surfaces as lining cells, or undergo apoptosis.

Osteoblast differentiation is controlled by several signaling pathways including but not limited to bone morphogenetic protein (BMP), Wnt, parathyroid hormone (PTH) transforming growth factor β (TGF- β), and Hedgehog (HH)^{45,46}.

Downstream of these signaling cascades are transcription factors that guide an osteoblast transitioning through the various differentiation steps. Among the most critical transcription factors is the Runt-related transcription factor 2 (RUNX2), which is considered the central regulator of osteoblast differentiation^{46,47}. For instance, in humans, loss-of-function mutation of the RUNX2 gene causes cleidocranial

dysplasia⁴⁸. Lack of RUNX2 in mice causes failure of the skeleton to mineralize due to an early stage block of osteoblast differentiation⁴⁹. However, RUNX2 has been thought to play a negative role at terminal differentiation stages, since overexpression of RUNX2 blocks late-stage osteoblast function^{50,51}. To regulate osteoblast differentiation, RUNX2 binds to specific DNA sequences and promotes the expression of osteoblast-related genes. In the promoter of the osteocalcin (OCN) gene, two cis-acting elements have been proved as RUNX2 binding sequences⁵². Other osteoblast-related genes such as COL1A1, ALP, and osteopontin also bear RUNX2 binding sequences in their promoters⁵³. In addition, RUNX2 regulates osteoblast differentiation through other transcription factors like osterix and activating transcription factor 4 (ATF4)^{54,55}.

OCN is the most abundant non-collagen protein in the bone matrix solely secreted by osteoblasts⁵⁶. The OCN protein contains a vitamin-K-dependent carboxylic γ -glutamic domain that aligns its residues with calcium ions in hydroxyapatite⁵⁷. After resorption in the matrix, OCN is decarboxylated and released into circulation. Hence, OCN in serum is considered as an indicator of bone formation and serves as a bone turnover marker in the clinics⁵⁸. However, some controversial evidence indicated that OCN is a negative regulator of bone formation since OCN knockout mice exhibited an increased bone formation with an unchanged bone resorption phenotype compared to wild-type mice⁵⁹. Moreover, OCN has been thought to regulate glucose metabolism, brain development, cognition, and male fertility in circulation as a hormone⁶⁰. However, these findings are discussed controversially in the field and no conclusion has been reached.

Osteoblast differentiation and function are important for reaching and maintaining a proper bone mass. In aged individuals, bone formation is reduced in part because of a decreased osteoblast differentiation and function, which contributes to low bone mass and ultimately osteoporosis⁶¹. In contrast, osteosclerosis is a condition with an increased bone mass due to an augmented osteoblast function^{62,63}.

1.3.2 Adipocyte differentiation

As mentioned, MSCs can also differentiate into adipocytes. After commitment, pre-adipocytes accumulate lipid droplets and adopt the phenotype of mature adipocytes.

Different signaling cascades including TGF- β , BMP, Insulin-like growth factor 1 (IGF1), and fibroblast growth factor (FGF) are involved in the process of adipocyte differentiation. However, in contrast to osteoblast differentiation, canonical Wnt and HH signaling are attenuated to facilitate adipocyte differentiation⁶⁴.

Downstream of the signaling pathways that govern adipocyte differentiation are transcription factors, which execute gene regulatory programs. CAAT/enhancer-binding proteins (C/EBPs) are a group of transcription factors known to regulate adipocyte differentiation. To adopt an adipocyte phenotype, C/EBP β and C/EBP δ are activated. These two factors increase the expression of the downstream factors C/EBP α and peroxisome proliferator-activated receptor γ (PPAR γ). The transcription factors PPAR γ and C/EBP α then associate with promoter regions of adipocyte-related genes and increase their transcription⁶⁵. In addition, both factors are subject to a mutual positive feed-forward loop, which might accelerate adipocyte differentiation (Fig. 1.6)⁶⁶.

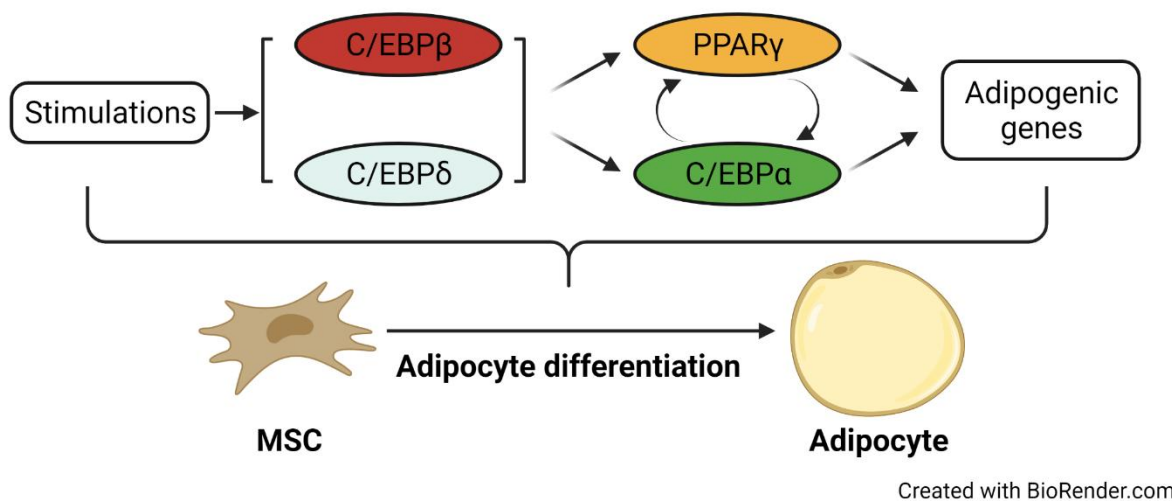


Figure 1.6. Transcriptional regulation of adipocyte differentiation. Stimulation of adipocyte differentiation increases the transcriptional activity of C/EBP β and C/EBP δ . This causes an increased abundance of C/EBP α and PPAR γ , which form an autoregulatory loop and increase the expression of adipocyte-related genes.

In the context of adipocyte differentiation, PPAR γ is firmly established as the master transcriptional regulator. Germline deletion of PPAR γ in mice is lethal at embryonic stages due to its critical role in placenta development. However, this lethal phenotype can be restored by supplementing PPAR γ via wild-type placentas but surviving

animals die within four months due to abnormal adipogenesis and multiple hemorrhages⁶⁷. In the context of postnatal targeted deletion of PPAR γ in mice using tamoxifen-dependent Cre-Lox recombination, PPAR γ ^{-/-} adipocytes vanished in a few days and were replaced by newly generated PPAR γ ^{+/+} adipocytes⁶⁸. That indicates that adipocyte differentiation may not be achieved without PPAR γ .

Due to the alternative use of promoters, PPAR γ exists in two isoforms: PPAR γ 1 and PPAR γ 2. PPAR γ 2 is the longer isoform with 28 extra amino acids at the N-terminus because of an earlier start codon⁶⁹. Distributions of these two isoforms are different. PPAR γ 1 is widely observed in many different tissues while PPAR γ 2 is only expressed in adipose tissue^{69,70}. Functionally, solely expressing PPAR γ 1 or PPAR γ 2 is sufficient to facilitate adipocyte differentiation in PPAR γ -null 3T3-L1 cells. However, compared with PPAR γ 1, only expressing PPAR γ 2 can achieve differentiation in less stimulation conditions⁷¹.

Fatty acids act as the energy source and signaling molecule but trafficking inside cells requires binding to proteins. In humans, fatty acid-binding protein (FABP) comprises 9 family members, which are tissue-specific (FABP1 in the liver, FABP3 and FABP7 in the brain)⁷². FABP4 is adipose tissue-specific and highly expressed in mature adipocytes. Because of sequence similarity with myelin P2, FABP4 is also known as adipocyte P2 (aP2)⁷³. A PPAR γ binding sequence is located in the promoter of FABP4 and expression of FABP4 is induced by PPAR γ agonists^{74,75}.

Adiponectin (ADIPOQ) is another adipocyte marker gene. Binding with its receptors, ADIPOQ in serum regulates glucose and lipid metabolism by decreasing insulin sensitivity and is considered as a negative regulator of obesity⁷⁶. ADIPOQ is essential for adipogenesis since silencing ADIPOQ expression by shRNA impaired adipocyte differentiation⁷⁷. Like FABP4, expression of ADIPOQ is also regulated by PPAR γ . A putative binding sequence is detected in both human and mouse promoters⁷⁸. A decreased expression of ADIPOQ was observed in adipose tissue-targeted deficiency of PPAR γ in mice⁷⁹.

Adipocyte differentiation is related with lipid metabolism. Abnormal adipogenesis is observed in many diseases like type 2 diabetes, hepatic steatosis, and hypertriglyceridemia⁸⁰. Regarding bone mass, adipocytes are reported as negative regulators of osteoblast differentiation. In addition, factors secreted by

adipocytes like leptin, ADIPOQ, resistin and visfatin promote osteoclast differentiation and bone resorption activity^{81,82}.

1.3.3 Epigenetic modifications in MSCs differentiation

MSCs differentiation is also controlled by epigenetic modifications. For example, DNA methylation comprises the addition of a methyl group to DNA, which commonly occurs on cytosine-phosphate-guanine dinucleotides. As a result, DNA methylation of the promoter inhibits the expression of the respective gene⁸³. Villagra et al. reported that reduced methylation of the OCN promoter was observed during osteoblast differentiation⁸⁴. Consistently, PPAR γ promoter methylation decreases adipogenesis⁸⁵. Another well-studied epigenetic regulation is histone modifications. Histones are eukaryotic small proteins rich in lysine and arginine, which act as spools for DNA winding⁸⁶. Modifications of histones including methylation, phosphorylation, acetylation, and ubiquitylation have the potential to increase or decrease gene expression^{86,87}. For instance, methylation of lysine 27 on histone H3 (H3K27me3) enhances MSCs differentiation into osteoblasts while decreasing differentiation into adipocytes. However, demethylation of H3K27me3 regulates MSCs differentiation in the opposite way^{88,89}.

1.4 Adenosine deaminase on double-strand RNA (ADAR)

RNA editing comprises the modification of the chemical structure of RNA molecules, which is a form of post-transcriptional epigenetic regulation⁹⁰. The process of RNA editing is common and evolutionarily conserved across many species up to humans. Sorted by consequence, RNA editing comprises insertion, deletion, or substitution of nucleotides⁹¹.

Adenosine deaminase on double-strand RNA (ADAR) is an important RNA editing enzyme converting adenosine to inosine (A-to-I) (Fig. 1.7.A). Inosine (I) has a similar molecular structure to guanosine (G), inosine can base-pair with cytidine (C). At the transcriptional level, this pairing can be considered as an A-to-G switch (Fig. 1.7.B&C)^{92,93}.

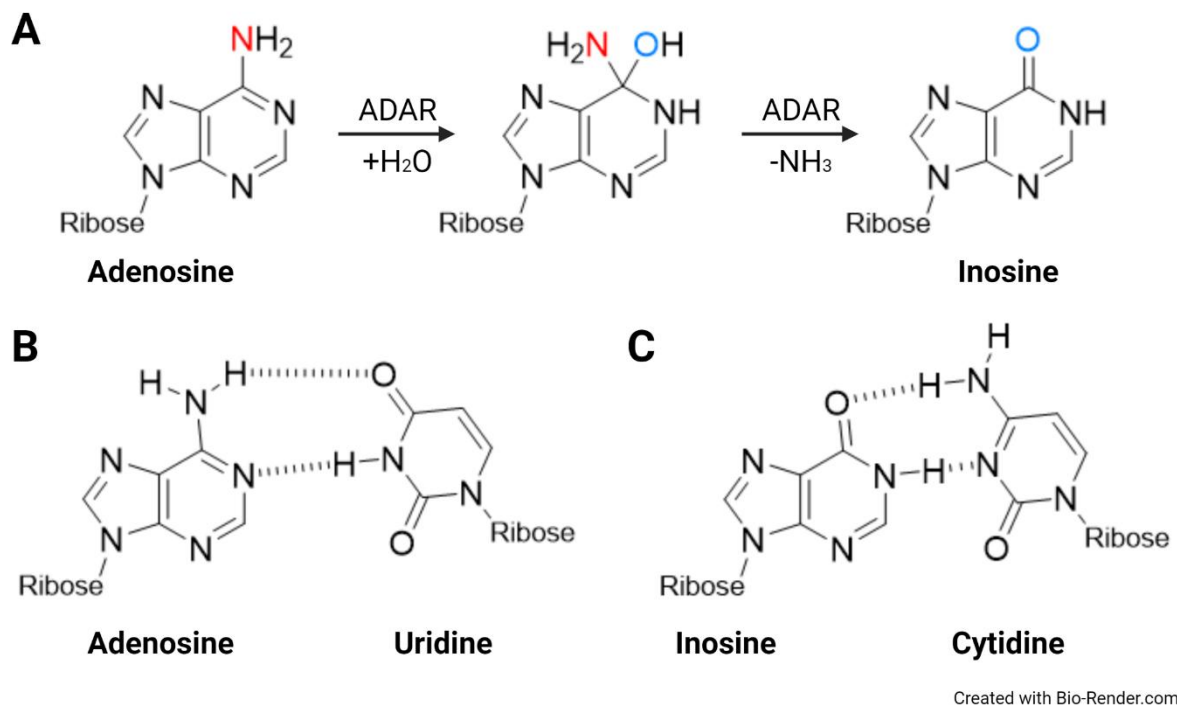
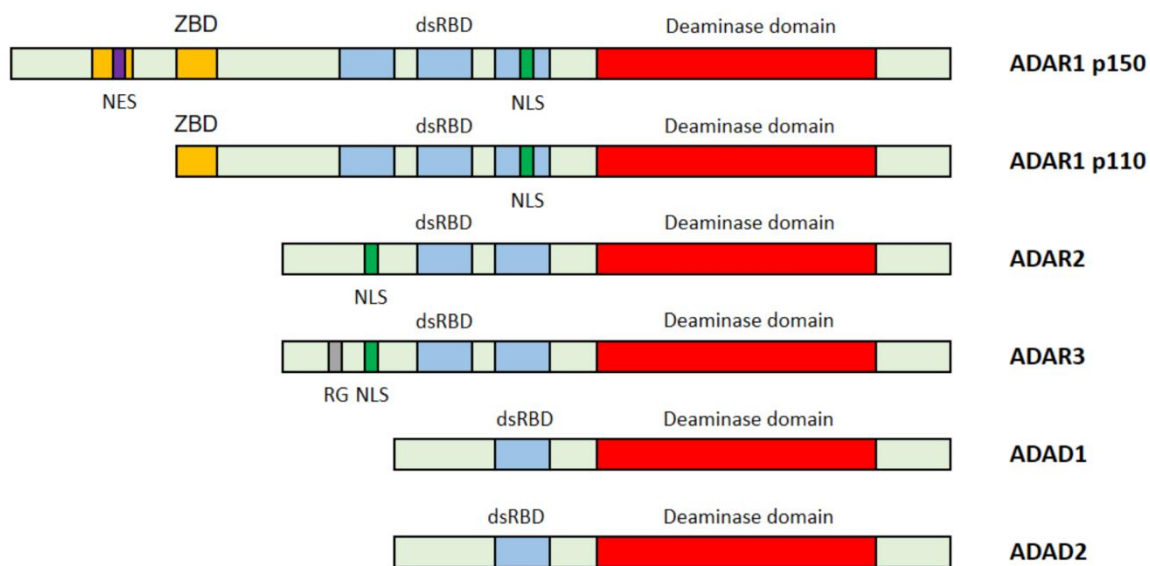


Figure 1.7. Schematic of ADAR-mediated adenosine deamination. **A** ADAR-dependent deamination of adenosine involves an intermediate stage in which a hydroxy group is added at position 9 of purine. During the conversion into inosine, an ammonia group is removed. **B** Adenosine naturally forms base-pairing with uridine. **C** After deamination, the newly generated inosine forms base-pairing with cytidine.

1.4.1 Members of the ADAR family

In mammals, the ADAR family comprises five members: ADAR1, ADAR2, ADAR3, and adenosine deaminase domain (ADAD)-containing genes ADAD1 and ADAD2^{94,95}. In humans, 2 isoforms of ADAR1 exist: a full-length p150 isoform and a shorter length p110 isoform^{96,97}. All ADAR family members have a similar structure, including a C-terminal deaminase domain and different numbers of dsRNA binding domain (dsRBD). Both isoforms of ADAR1 contain a specific Z-DNA binding domain (ZBD) (Fig. 1.8).



Created with Bio-Render.com

Figure 1.8. Structure of ADAR family members. All ADAR family members have a similar domain structure with a deaminase domain (red) at the C-terminal end and a variable number of dsRNA-binding domains (dsRBD) (blue). ADAR1 (both p150 and p110) contains Z-DNA binding domain (ZBD). ADAR1, ADAR2, and ADAR3 bear a nuclear localization sequence (NLS) (green). In particular ADAR1 p150 includes a nuclear export sequence (NES) (purple) at the N-terminus. ADAR3 comprises an arginine-glycine-rich region on its N-terminus (RG) (gray) that can interact with RNA.

Among family members, only ADAR1 and ADAR2 are proved to contain deamination enzyme activity and express widely in all types of tissues. Inside the cell, ADAR2 and ADAR1 p110 are mainly localized in the nucleus, while ADAR1 p150 is present in the nucleus and the cytoplasm⁹⁸. ADAR3, however, is only detected in the central nervous system with no enzyme activity and is therefore considered as a competitive inhibitor of ADAR1 and ADAR2⁹⁹. The remaining two family members, ADAD1 and ADAD2, are testis-specific without deamination activity and regulate male germ cell differentiation⁹⁵.

1.4.2 Editing mechanism and selectivity

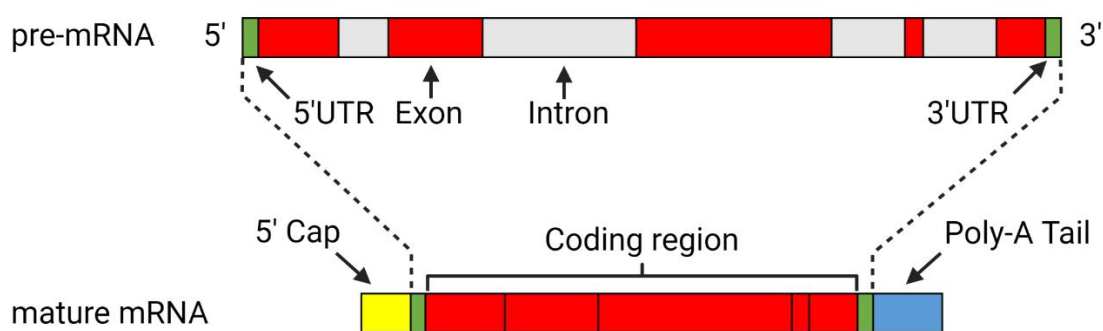
To perform A-to-I editing, ADAR first interacts with double-stranded RNA using its dsRBD. Then, the deaminase domain flips the target base out of the double helix and mediates deamination of the nucleotide¹⁰⁰. It is known that A-to-I editing enzyme activity requires homo-dimerization of ADAR. ADAR1 and ADAR2 were confirmed to

form homo-dimer *in vitro* and *in vivo*^{101,102}. ADAR3, however, lacks this ability, which might be the reason for its enzyme inactivity¹⁰².

A-to-I RNA editing mediated by ADARs only occurs in the context of a double-strand structure. Both inter- and intra-molecular dsRNA with perfect or un-perfect pairing can be recognized as substrates¹⁰³. In long-chain dsRNA with perfect pairing, A-to-I editing is non-specific. Adenosine deamination is likely to decrease the stability of the double-strand structure. Thus, editing continues until the double-strand structure does no longer exists. By contrast, short dsRNA or imperfect matched dsRNA, bulges, and loops are edited selectively: only a few adenosines are edited specifically¹⁰⁴. The reason for ADAR editing selectivity is still unclear.

1.4.3 Functional implication of A-to-I editing

Messenger RNA (mRNA), the most abundant type of RNA in cells, directs the synthesis of protein. Transcribed from DNA, pre-mRNA contains both coding (exons) and non-coding (introns and untranslated regions on 5' and 3') sequences. After transcription, pre-mRNA undergoes many modifications in the nucleus like splicing, 5' capping, and 3' poly-A tail adding. After that, mature mRNA can be exported into the cytoplasm to serve as the template for protein translation. In mature mRNA, exons are linked together and form the coding region that encodes a protein (Fig. 1.9)¹⁰⁵.



Created with Bio-Render.com

Figure 1.9. mRNA processing. From pre- to mature mRNA, processing includes splicing, 5' capping, and 3' poly-A tail adding. Introns represent the non-coding sequence between exons, which are excised during splicing. After that, all exons are directly connected as a coding region. Both 5' and 3' ends of the mRNA represent untranslated regions (UTRs). UTRs exist in mature mRNA without translation function.

ADAR-mediated A-to-I editing implicates the function of mRNA via direct and indirect manners. If A-to-I editing occurs in exons, the function of protein is changed by direct codon sequence alteration. The most well-understood example is on the subunit of ionotropic α -amino-3-hydroxy-5-methyl-4-isoxazolepropionic acid (AMPA) glutamate receptor. In mammals, the AMPA receptor is constituted by 4 subunits named GRIA1 to GRIA4 separately¹⁰⁶. The A-to-I editing event occurring on exon 11 of GRIA2 shifts the amino acid from glutamine (Q) to arginine (R), hence the editing site is named as GRIA2 Q/R site. This editing event is exclusively mediated by ADAR2, which leads to the functional change of AMPA receptor from Ca^{2+} -permeable into impermeable (Fig. 1.10)¹⁰⁷. A-to-I editing of the GRIA2 Q/R site is critical since AMPA receptor with unedited GRIA2 subunit leads to severe seizures. That is the main reason why mice bearing a germline deletion of ADAR2 (ADAR^{-/-}) die at a very young age and introducing an edited version of GRIA2 (GRIA2^{R/R}) prevents this lethal phenotype¹⁰⁸.

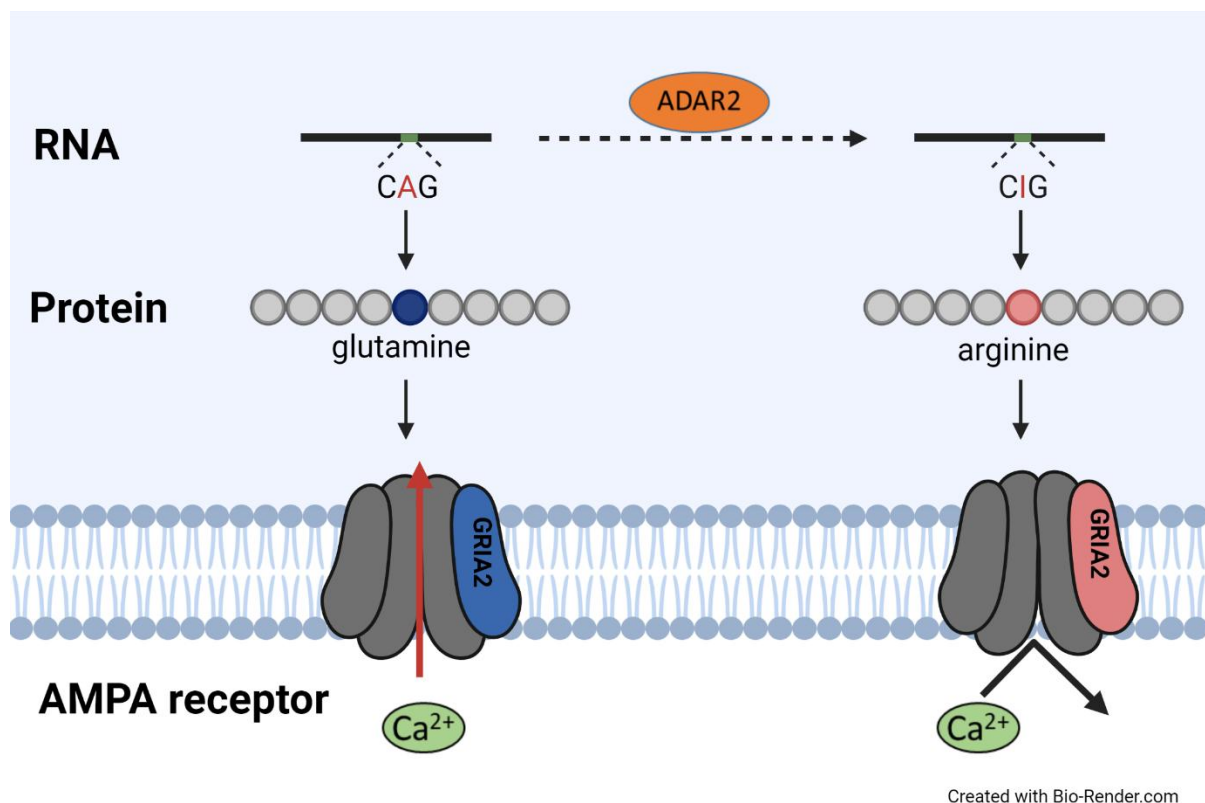


Figure 1.10. ADAR2-mediated editing of GRIA2. ADAR2 is known as the only family member mediating A-to-I editing in the exon of GRIA2, which leads to the conversion of amino acids from glutamine (codon CAG) to arginine (codon CIG). As a result, AMPA receptor with unedited GRIA2 allows Ca^{2+} influx, while AMPA receptor with edited GRIA2 is Ca^{2+} -impermeable.

Additionally, A-to-I editing in exons may also lead to the generation or exclusion of stop codons and consequently to a hypomorph with a gain- or loss-of-function. There are 3 types of stop codons at the RNA level: amber (UAG), ochre (UAA), and opal (UGA). A Japanese group confirmed that artificially designed ADAR1 converted all these stop codons into amino acid-coding codons^{109,110}.

Besides occurring in exons, A-to-I editing is more frequent in introns and non-coding regions. The possible reason is that these regions contain more dsRNA. The non-exon transcriptome contains numerous Alu elements (a type of short interspersed retro-transposable element), which are more likely to form a double-strand structure¹¹¹. A study by Licht et al. identified around 90,000 unknown A-to-I editing events in the mouse brain transcriptome using Nascent-seq. The manuscript reported that editing in exons only accounted for a small part of all editing events¹¹². Consistently, in humans, most A-to-I editing occurs outside exon regions mainly in Alu elements^{113–116}.

A-to-I editing events in introns and other non-coding regions lead to alternative splicing of mRNA. By A-to-I editing, the 5' splicing site (GU) can be generated. Similarly, the 3' splicing site (AG) can be both generated or eliminated¹¹⁷. For example, ADAR2 self-editing of its pre-mRNA creates a 3' splice site (AA to AI) in intron 4 (Fig. 1.11.A)¹¹⁸. A-to-I editing also affects mRNA nuclear localization. Prasanth et al. reported that editing events within the 3' UTR of mouse cationic amino acid transporter 2 transcribed nuclear RNA (CTN-RNA) trap itself inside the nucleus by binding to P54^{nrb} (a nuclear retention protein) (Fig. 1.11.B)¹¹⁹.

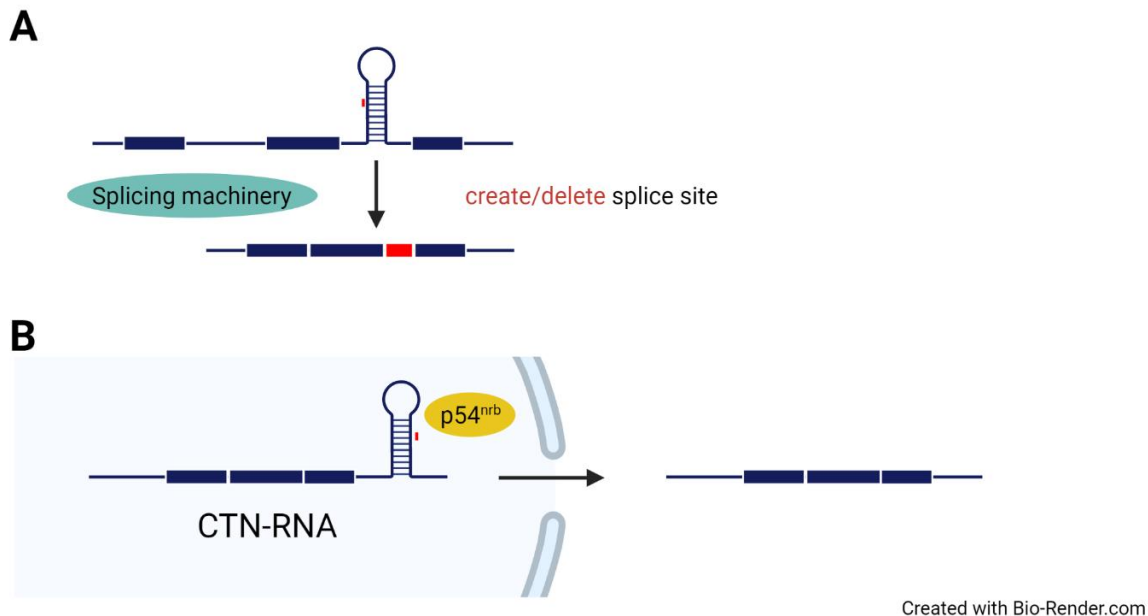


Figure 1.11. A-to-I editing of RNA non-coding regions. **A** A-to-I editing creates or deletes splicing sites, which leads to the insertion or elimination of sequences. **B** A-to-I editing affects RNA localization. Cationic amino acid transporter 2 transcribed nuclear RNA (CTN-RNA) entraps itself inside the nucleus by binding to p54^{nrb}. This binding sequence is generated by ADAR-related A-to-I editing⁹³.

ADARs mediated A-to-I editing also interacts with micro-RNA (miRNA) function. miRNAs are a group of small non-coding RNA (around 22nt long). Binding to their target sequence, miRNAs regulate the degradation or translation of target mRNAs. miRNA is generated by Dicer using long dsRNA as the template. Hence, only well-edited dsRNA can be spliced into miRNA¹²⁰. Additionally, the binding sites of miRNA were reported to be modified by ADAR¹²¹.

1.4.4 ADAR-related diseases

Aberrant ADAR function can cause severe disorders in the central nervous- and immune system. For example, a variety of ADAR1 mutations are observed in patients with Aicardi–Goutières syndrome (AGS), an early onset inherited disease, characterized by bilateral striatal necrosis in the brain¹²². Another condition is the skin disease Dyschromatosis symmetrica hereditaria (DSH), which is associated with non-functional ADAR1¹²³. Likewise, patients bearing a mutation of ADAR2 have suffered from microcephaly with intellectual disability and epilepsy¹²⁴.

Clinical relevance of hyper- or hypo-editing events is provided by observations made in the context of cancer progression. For instance, in hepatocellular carcinoma

A-to-I editing of antizyme inhibitor 1 is increased¹²⁵. In addition, a transcriptome analysis identified a higher editing frequency in breast cancer tissue compared with normal tissue¹²⁶. Furthermore, ADAR1 was observed to promote leukemia progression¹²⁷. In contrast, enforced expression of ADAR2 inhibits glioblastoma cell proliferation and migration¹²⁸.

2. Hypothesis

2.1 Hypothesis

Bone tissue is highly dynamic with a continuous remodeling to maintain bone mass. MSCs contribute to bone mass maintenance by differentiating into osteoblasts and adipocytes. Therefore, further elucidating the mechanism by which MSCs differentiate into those cell types is very important to better understand processes preserving bone health. Ongoing original research project in our laboratory collected and investigated femoral head samples of aged people, which contain abundant fat tissue. Sequencing analyses suggested a high expression of ADAR2 in low bone mass samples because of an intensive H3K27ac of its promoter region. Hence, we hypothesized that ADAR2 plays an important role in MSCs differentiation towards osteoblasts and/or adipocytes. Testing this novel hypothesis is subject of this doctoral thesis.

2.2 Aims

To test the hypothesis that ADAR2 is functionally relevant in MSCs differentiation, the following specific aims will be conducted:

Aim 1: Determine ADAR2 expression during MSC differentiation

Aim 2: Characterize the differentiation phenotypes upon ADAR2 inhibition

Aim 3: Investigate the mechanism of ADAR2-dependent MSC differentiation

3. Material and Methods

3.1 Chemicals, equipment, and consumables

Table 3.1 List of chemicals used

Chemical	Manufacturer
0.05% Trypsin-EDTA (1X)	Gibco
0.25% Sodium-deoxycholate	Merck
10x Tris/Glycine/SDS Buffer	Bio-Rad
1-bromo-3-chloropropane	Sigma
1 α ,25-dihydroxy vitamin D3	Sigma
2% Alizarin Red S (pH 4.2)	ScienCell
2-Propanol	Roth
3-isobutyl-1-methylxanthine (IBMX)	Sigma
4x Laemmli Sample Buffer	Bio-Rad
6x TriTrack DNA Loading Dye	Thermo Scientific
Acetic acid	Roth
Acrylamide/Bisacrylamide (Rotiphorese(R) Gel 30) (37, 5:1)	Roth
Ammonium persulfate (APS)	PanReac Applichem
Complete Tablets, Protease Inhibitor cocktail tablets	Roche
Dexamethasone	Sigma
Dulbecco's Modified Eagle Medium (DMEM) [+] 4.5 g/L D-Glucose, L-Glutamine [+] pyruvate	Gibco
Ethylenedinitrilotetraacetic acid (EDTA), disodium salt dihydrate	Merck
Fast Blue RR salt	Sigma
Fetal bovine serum (FBS)	Anprotec
Formaldehyde solution min. 37% free from acid	Merck

GeneRuler DNA Ladder Mix	Thermo Scientific	
Glycine	Sigma	
Precision Protein StrepTactin-HRP Conjugate	Bio-Rad	
Hydrochloric Acid (HCl)	Merck	
Insulin, recombinant Human	SAFC Biosciences	
L-Ascorbic Acid	Sigma	
Methanol	Honeywell	
Midori Green	NIPPON Genetic	
N,N,N',N'-Tetramethylethylenediamine (TEMED)	Sigma	
N,N-Dimethylformamide	Sigma	
Naphthol AS-MX phosphate disodium salt	Sigma-Aldrich	
Nonidet P-40 Substitute	Sigma	
Oil red O	Sigma-Aldrich	
Penicillin/Streptomycin (P/S)	Gibco	
Phosphate Buffered Saline (PBS) pH 7.4	Gibco	
Phosphate Buffered Saline (PBS) powder pH 7.4	Sigma	
PhosSTOP, Phosphatase Inhibitor cocktail tablets	Roche	
Ponceau S, 0.2% v/v soln. in 5% acetic acid	Alfa Aesar	
Powdered Milk	Roth	
Precision Plus Protein™ WesternC™ Blotting Standards	Bio-Rad	
Rosiglitazone	EMD Millipore Corp	
Sodium Chloride (NaCl)	Merck	
Sodium dodecyl sulfate (SDS) Pellet	Roth	
SYBR™ select master Mix for CFX (SYBR Green)	Thermo Scientific	Fisher
TRI reagent (Trizol)	Sigma	

Trizma® Base (Tris base)	Sigma
Trizma® Hydrochloride (Tris HCl)	Sigma
Trypan Blue	Sigma
Tween 20®	PanReac Applichem
Water (nuclease free)	Sigma
β-glycerolphosphate disodium salt pentahydrate	Sigma

Table 3.2 List of equipment used

Equipment	Model	Company
Centrifuge	5425/5920R	Eppendorf
Cell counter	TC20 Automated	Bio-Rad
Clean bench	HERASAFE 2030i	Thermo Scientific
Electrophoresis chamber	Mini-PROTEAN Tetra Handcast system	Bio-Rad
Imager	ChemiDoc MP Imaging system	Bio-Rad
Incubator	CellXpert C170i	Thermo Scientific
Microscope	Axiovert 40 CFL	Carl-Zeiss
Microscope (Fluorescent)	Axio Observer	Carl-Zeiss
Magnetic stirrer	Hei-Standard	Heidolph
Spectrophotometer	NanoDrop One	Thermo Scientific
Microplate reader	VICTOR Nivo Multimode	Perkin Elmer
pH meter	FiveEasy Standard	Mettler Toledo
Pipettes	Research Plus	Eppendorf
Scanner	Perfection V850 Pro	Epson
Orbital-rocking Shaker	3012	GFL
Thermocycler	C1000 Touch	Bio-Rad

Thermocycler Realtime PCR	CFX connect Real-time PCR Detection system	Bio-Rad
Transfer system	Trans-Blot Turbo	Bio-Rad
UV table	TFX-20 MX, high/low intensity	Thermo Scientific

Table 3.3 List of consumables used

Consumable	Company
Cell culture flask	BD Falcon™
Cell culture plate (6-well)	Sarstedt
Counting slide	Bio-Rad
Filter Paper	Whatman™, GE Healthcare Life Sciences
Nitrocellulose (NC) membrane	Peqlab
Pipette tips	Eppendorf, Tip one
qPCR Plate (96-well)	Bio-Rad
Tissue culture Flask T175	Sarstedt
Tubes	Eppendorf

3.2 Kits

Table 3.4 List of Kits used

Kits	Company
RNeasy® Plus Mini Kit	QIAGEN
Verso cDNA synthesis	Thermo Scientific
Lipofectamine® 3000 Transfection Kit	Invitrogen
Clarity™ Western ECL Substrate	Bio-Rad
SuperSignal™ West Femto Maximum Sensitivity Substrate	Thermo Scientific
Pierce™ BCA Protein Assay Kit	Thermo Scientific

SuperScript™ IV One-Step system with ezDNase™ Enzyme Kit	Thermo Scientific
QIAquick Gel extraction Kit	QIAGEN

3.3 Oligonucleotides

All oligonucleotides were custom designed and obtained from Eurofins MWG.

Table 3.5 List of oligonucleotides used

Name	Oligonucleotide 5'-3'	Application
hGAPDH-F	GTCTCCTCTGACTTCAACAGCG	qRT-PCR
hGAPDH-R	ACCACCCTGTTGCTGTAGCCAA	qRT-PCR
hADARB1-F	CCCTCACGCTCGCAGAAAAG	qRT-PCR
hADARB1-R	GCAGTCATTTAATGCAAGGCCACG	qRT-PCR
hFABP4-F	CATACTGGGCCAGGAATTTGAC	qRT-PCR
hFABP4-R	GCTCTCTCATAAACTCTCGTGG	qRT-PCR
h PPAR γ -F	CATGCTTGTGAAGGATGCAAGG	qRT-PCR
h PPAR γ -R	CTTCTCCTTCTCGGCCTGTG	qRT-PCR
hADIPOQ-F	GACGGGATTTACCCATGTTGTC	qRT-PCR
hADIPOQ-R	GATGCCCGCCATCCAACCTGT	qRT-PCR
hADAR1-F	CTCCCAGACTGCGAAGGATAG	qRT-PCR
hADAR1-R	CGGAGCTTTCCTTGTTTGGG	qRT-PCR
hRUNX2-F	GTTACTGTCATGGCGGGTAAC	qRT-PCR
hRUNX2-R	GATAGGTAGCTACTTGGGGAGG	qRT-PCR
hOCN-F	CCATGAGAGCCCTCACACTC	qRT-PCR
hOCN-R	GGGCTCCCAGCCATTGATAC	qRT-PCR
hGRIA2 Q/R-F	GCACACTGAGGAGTTTGAAGATG	Sequencing
hGRIA2 Q/R-R	GCTAAGTTAGCCGTGTAGGAGG	Sequencing

3.4 Antibodies

Table 3.6 List of antibodies used

Antibody	Binding type	Host	Dilution	Company
Actin	Primary	Mouse	1:4,000	Sigma
ADAR2	Primary	Rabbit	1:500	Biorbyt (Biol)
Anti mouse IgG	Secondary	Goat	1:10,000	Bio-Rad
Anti rabbit IgG	Secondary	Goat	1:10,000	Bio-Rad

3.5 siRNA

Table 3.7 List of siRNA used

siRNA	Company
ON-TARGETplus Non-targeting Pool	Dharmacon
ON-TARGETplus Human ADARB1 siRNA-SMARTpool	Dharmacon

3.6 Software

Table 3.8 List of software used

Software	Company
BioRender	BioRender
CFX Manager	Bio-Rad Laboratories
Chromas 2.6.6	Technelysium
Image Lab 6.1	Bio-Rad Laboratories
Microsoft Office 2016	Microsoft Corp.
Serial Cloner 2.6.1	Serial Basics
ZEN 2012 (blue edition)	Zeiss
Image J 1.8.0	National Institutes of Health (NIH)

3.7 Cell culture

3.7.1 Cell line

Telomerase reverse transcriptase (TERT) transduction allows cells to acquire unlimited proliferation ability. The cell line of TERT transduced human mesenchymal stem cell (hMSC-TERT) was first generated by Simonsen, which had a normal karyotype and the ability to proliferate without forming tumors¹²⁹. This cell line has been proved to differentiate into osteoblast and adipocyte *in vitro* by Rauch et al¹³⁰. In this study, hMSC-TERTs were at passage 37 to 48 and cells were kindly provided by Dr. Kassem from Odense, Denmark.

3.7.2 Culture conditions

hMSC-TERTs cells were cultured in Dulbecco's Modified Eagle Medium (DMEM) containing nucleosides, 10% fetal bovine serum (FBS), and 1% Penicillin/Streptomycin (P/S). Cells proliferated in tissue culture flasks at 37°C, 5% CO₂, and 95% relative humidity in the incubator (Thermo Scientific). The culture medium was changed every 2 to 3 days.

3.7.3 Cell culture passaging

Cell layers were trypsinized at 80% confluence. Adherent cells were washed twice with 1x phosphate-buffered saline (PBS) and incubated with Trypsin-EDTA solution for 5 minutes at 37°C, 5% CO₂, and 95% relative humidity in the incubator (Thermo Scientific) for enzymatic release of the sub-confluent cell layer. The reaction was stopped by fresh DMEM containing 10% FBS and 1% P/S. Released cells were centrifuged at 180x g at room temperature for 5 minutes. After centrifugation, cells had formed a pellet on the bottom of the tube. The cell pellet was re-suspended in the culture medium, followed by cell counting and seeding in 6-well plates or in culture flasks.

3.7.4 Cell counting

To count the number of cells, 10µl cell suspension and 10µl Trypan blue were mixed in a tube. The mixture was pipetted onto a counting slide. Cells were counted automatically using a cell counter (Bio-Rad).

3.7.5 Cell differentiation

To induce osteoblast differentiation, a differentiation medium containing the following supplements was used:

Osteoblast differentiation medium

DMEM with 10% FBS and 1% P/S

Ascorbic Acid	50 µg/µl
β-glycerophosphate	10 nM
1,25-dihydroxy Vitamin D3	10 nM
Dexamethasone	10 nM

To induce adipocyte differentiation, a differentiation medium containing the following supplements was used:

Adipocyte differentiation medium

DMEM with 10% FBS and 1% P/S

Insulin	10 µg/ml
3-isobutyl-1-methylxanthine (IBMX)	50 nM
Rosiglitazone	1 µM
Dexamethasone	100 nM

hMSC-TERTs were seeded in 6-well plates at a concentration of 2×10^5 cells/well. Cell differentiation was induced by treating cells with osteoblast- or adipocyte differentiation medium (ingredients listed above). The day when the differentiation medium was provided was considered as day 0. Differentiating cells were cultured at 37°C, 5% CO₂, and 95% relative humidity. Osteoblast differentiation was completed by day 28. Adipocyte differentiation was completed by day 21. The differentiation medium was changed every 2 to 3 days.

3.8 Transient transfection

Transient transfection is a process by which exogenous nucleic acids are introduced into eukaryotic cells to achieve a temporary effect. Small interfering RNA (siRNA) is a class of non-coding double-stranded RNA. siRNA transfection interferes with the expression of specific genes.

In this study, siRNAs were transiently transfected by a chemical-based method using Lipofectamine 3000 (Invitrogen). siRNA transfection was performed in 6-well plates 1 day prior to stimulation of cells and during the stimulation process. Transient transfections were performed on adherent cell layers at a confluence of 70 to 80%. Briefly, 5 μ l siRNA (20 μ M) and 7.5 μ l reagent Lipofectamine 3000 were mixed in 125 μ l DMEM without FBS. After incubation at room temperature for 10 minutes, a complex had formed and the 250 μ l mixture was transferred onto the cell layer. Cells then continued incubating in the incubator (Thermo Scientific). After at least 8 hours, transient transfection was stopped by washing the cells with PBS and incubating the cells in the culture medium with or without differentiation supplements.

3.9 Staining methods

3.9.1 Alkaline phosphatase staining

Alkaline phosphatase (ALP) is widely expressed by different cells. In bone tissue, osteoblasts secrete ALP, which facilitates extracellular matrix mineralization. ALP is considered as a marker gene of osteoblast differentiation. The formula of the ALP staining solution is indicated below:

ALP Staining solution

1 M Tris-HCl (pH 8.4)	5 ml
Distilled water	45 ml
AS-MX phosphate disodium salt	5 mg
N,N-Dimethylformamide	200 μ l
Fast Blue RR salt	30 mg

Because ALP staining solution is not stable, it is prepared freshly and used immediately. First, Naphthol AS-MX phosphate disodium salt was dissolved in N,N-Dimethylformamide. This solution was then added into 0.1 M Tris-HCl (diluted by distilled water). Finally, Fast Blue RR salt was added to the mixture and vortexed carefully. After filtration, the staining solution was ready to use.

Before staining, cells were fixed with 3.7% formaldehyde diluted in 1x PBS for 15 minutes and rinsed twice with 1x PBS. Cells were then incubated with ALP staining solution in the dark at room temperature for 15 minutes. Stained cells were rinsed with distilled water and air-dried. Culture plates were scanned using a scanner (Epson).

3.9.2 Alizarin red staining

Alizarin red staining is frequently used to visualize mineralized extracellular matrix. In this study, a 2% Alizarin Red S ready-to-use staining solution (pH 4.2) was used. For fixation, cells were treated with 3.7% formaldehyde diluted in 1x PBS for 15 minutes and rinsed twice with 1x PBS. Then, the Alizarin Red S staining solution was added to each well. Plates were incubated at room temperature for 20 minutes. To reduce the background stain, stained cells were washed with distilled water while shaking gently and then air-dried. Cell culture plates were scanned using a scanner (Epson).

3.9.3 Oil red O staining

Mature adipocytes contain lipid droplets. Oil red O is a lysochrome diazo dye that was used for lipid droplet staining with red fluorescent¹³¹. The formula of oil red O staining solution is indicated below:

Oil red O stock solution

Oil red O	0.5 g
2-propanol	100 ml

Oil red O staining solution was prepared freshly by diluting the stock solution with distilled water at a ratio of 3:2.

Prior to oil red O staining, cells were fixed with 3.7% formaldehyde diluted in 1x PBS for 15 minutes and washed twice with 1x PBS. For staining, the cell layer was gently washed with running tap water for at least 1 minute. Cells were rinsed using 60% 2-propanol (diluted with distilled water) and stained with oil red O working solution for at least 60 minutes. After removing the staining solution, cells were washed again under running tap water and kept moist. Stained cell layers were imaged using a microscope (Carl-Zeiss).

A fluorescent microscope (Carl-Zeiss) was used to obtain the large image of oil red O staining. The region of interest was set as 9.32mm x 9.32mm in the center of each well to capture most of the stained area. Phase contrast images were obtained as channel 1. Since oil red O has the character of fluorescence, red fluorescent images were also acquired to illustrate stained lipid droplets as channel 2. The full grayscale of these two channels was 0 (black) to 4095 (white). After adjusting of parameters, these 2 channels merged as the large image of oil red O staining (Fig. 3.1.A).

For quantification, the area of red fluorescence was measured as the relative indicator of adipocyte differentiation. Adjusted channel 2 in each well was exported as the fluorescent image. Image J then processed the fluorescent image by converting it into black and white and adjusting the threshold. After that, the white part area was measured automatically as the indicator (Fig. 3.2.B).

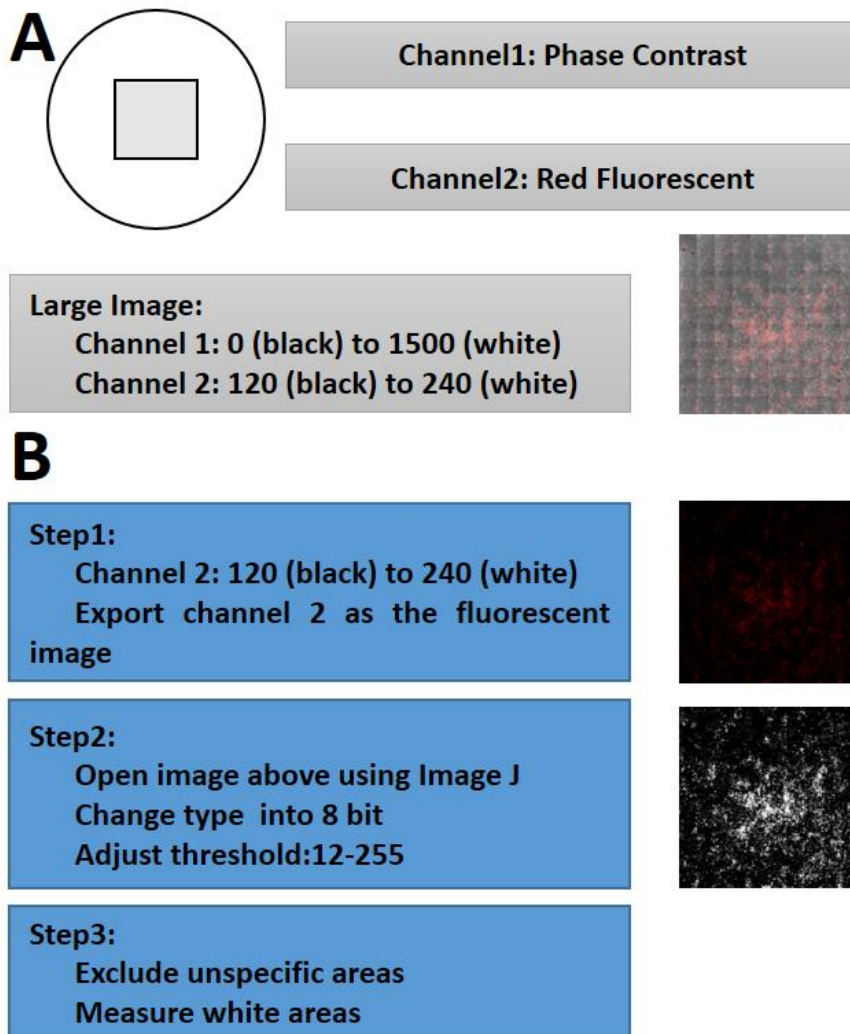


Figure 3.1: Workflow to obtain larger images of Oil red O-stained cell layers. **A:** The large image of Oil red O-stained cell layers were first obtained using phase contrast images (channel 1), which were then merged with images showing red fluorescence (channel 2). **B:** Red fluorescent images were subjected to quantification of cells that underwent adipocyte differentiation. Quantification was performed in three steps. In step 1, channel 2 with parameters ranging from 120 (black) to 240 (white) was exported as the fluorescent image (the upper picture). In step 2, the fluorescent image was changed into 8-bit images and the threshold was adjusted to 12-255. After that, fluorescent area appeared white in images (the lower picture). In step 3, the non-specific area was excluded manually, and the white area was measured automatically.

3.10 RNA isolation

3.10.1 RNeasy kit method

RNeasy Plus mini kit (QIAGEN) was used to extract RNA from differentiated osteoblasts. Cells were washed with 1x PBS and placed on ice immediately. 350µl Buffer RLT Plus (included in the kit) was added to each well. RNA was isolated according to the protocol provided by the manufacturer. Finally, RNA was dissolved in 30 µl RNase-free water. The RNA concentration of each sample was determined

using a spectrophotometer (Thermo Scientific). All RNA samples were stored at -80°C.

3.10.2 Trizol method

Unfortunately, the RNeasy Plus kit is not suitable to isolate high-quality RNA from adipocytes due to the high abundance of lipid droplets. RNA from adipocytes was therefore extracted using the Trizol procedure. After washing with 1x PBS, cells were lysed using 1 ml Trizol. After complete dissociation, cell lysate was transferred into 1.5 ml tubes and mixed with 100 µl 1-bromo-3-chloropropane. After shaking gently for 15 seconds, the solution was incubated at room temperature for 5 minutes. The mixture was centrifuged at 12,000x g for 15 minutes, leading to a separation into 3 phases: a red organic phase (containing proteins), an interphase (containing DNA), and a clear upper aqueous phase (containing RNA). The aqueous phase was transferred into a new tube and mixed with 2-propanol. After shaking gently for 15 seconds, the solution was incubated for 5 minutes. The mixture was centrifuged at 12,000x g for 10 minutes. RNA formed a pellet and precipitated at the bottom. After removing the supernatant, the RNA pellet was washed in 75% ethanol. Finally, the RNA pellet was dissolved in 30 µl RNase-free water. The RNA concentration of each sample was determined using a spectrophotometer (Thermo Scientific). All RNA samples were stored at -80°C.

3.11 cDNA synthesis

RNA is unstable for amplification because of its single strand structure. Complementary DNA (cDNA) is generated from RNA templates via reverse transcription. cDNA was synthesized using a verso cDNA synthesis Kit (Thermo Scientific). The amount of 1 µg RNA for each sample was diluted in 11 µl nuclease-free water. The components of each synthesis reaction mix are indicated below. The reaction mix was pipetted on ice.

cDNA synthesis reaction mix (20 µl)

5x cDNA synthesis buffer	4 µl
dNTP Mix	2 µl
Random Hexamers	1 µl

RT Enhancer	1 μ l
Enzyme Mix	1 μ l
RNA in nuclease-free water	11 μ l

The reaction was incubated in a Thermocycler (Bio-Rad) using the following program:

Step	Temperature	Time
1	42°C	30 min
2	95°C	2 min

After the program finished, cDNA was cooled down on ice, diluted 20x with nuclease-free water and stored at -20°C.

3.12 Quantitative real-time PCR (qPCR) analysis

qPCR is used to quantify the abundance of a specific cDNA. The procedure uses the Δ Ct method according to the Minimum Information for Publication of Quantitative Real-Time PCR Experiments (MIQE) guidelines, to determine relative expression. The threshold cycle Ct indicates the replication cycle at which the sample fluorescence exceeds the threshold. Comparing Ct values reveals differences in gene expression. In this study, quantification of the expression of the housekeeping gene human Glyceraldehyde 3-phosphate dehydrogenase (hGAPDH) was used as the internal control. The components of each reaction mix are listed below.

qPCR reaction mix (15 μ l)

cDNA solution	3 μ l
Nuclease-free water	3 μ l
Forward primer (10 μ M)	0.75 μ l
Reverse primer (10 μ M)	0.75 μ l
SYBR Green	7.5 μ l

The amplification was conducted using a Thermocycler Real-Time PCR (Bio-Rad). The cycle program is indicated below. Results were analyzed using the software CFX Manager.

qPCR cycle program

Step	Temperature	Time
1	95°C	3 min
2	95°C	30 s
3	57°C	30 s
4	72°C	30 s

Goto step 2, 39x

3.13 Immuno-blot analysis

3.13.1 Cell lysate preparation

Cell lysate was obtained using modified radio-immunoprecipitation assay (mRIPA) buffer (ingredients are shown below). 1x Protease inhibitors and 1x phosphatase inhibitors were added prior to use.

Modified radio-immunoprecipitation assay (mRIPA) buffer

Tris base	0.5 mM
Sodium chloride (NaCl)	150 mM
Nonidet P-40 (NP-40)	0.5%
Sodium-Deoxycholate	0.25%
Distilled water	up to 1L
Adjust pH to 7.5 with HCl	

For 6 well plates, 80 µl mRIPA buffer was added to each well after washing cells with 1x PBS. Cells were lysed on a shaker for 15 minutes. After centrifugation at 13,000g

for 15 minutes at 4°C, cell lysate was transferred into a 1.5 ml Eppendorf tube and stored at -80°C.

3.13.2 Quantification of protein concentration

Prior to gel electrophoresis, protein concentration was measured using a Pierce™ BCA protein assay kit (Thermo Scientific). To create a standard curve for subsequent quantification, bovine serum albumin (BSA) (provided by the kit) was diluted at concentrations of 0, 5, 10, 20, 40, and 80 µg/µl. BCA working solution was prepared by mixing BCA reagent A and reagent B at a ratio of 50:1. 100 µl working reagent was mixed with 100 µl of each BSA concentration or with protein samples of unknown concentration (dissolved 20x) in a 96 well-plate and incubated at 37°C for 30 minutes. Absorbance was measured at 560/10 nm for 500 ms using a microplate reader (Perkin Elmer). Concentrations of protein samples were quantified using a standard curve generated using the absorbance of the BSA standard samples.

3.13.3 Protein gel electrophoresis

The gel for protein electrophoresis consists of two parts: a separation gel at the bottom for separating proteins of different sizes and a stacking gel at the top for loading samples. The compositions of each gel are below:

<i>Separation Gel</i>		<i>Stacking Gel</i>	
Distilled water	3.5 ml	Distilled water	3 ml
Separation gel buffer	2.5 ml	Stacking gel buffer	1.25 ml
SDS solution (10%)	100 µl	SDS solution (10%)	50 µl
Acrylamide/Bisacrylamide	4 ml	Acrylamide/Bisacrylamide	650 µl
TEMED	5 µl	TEMED	5 µl
APS solution (10%)	50 µl	APS solution (10%)	25 µl

Separation Gel Buffer

1.5M Tris base pH 8.8 (adjust by HCl)

Stacking Gel Buffer

0.5M Tris base pH 6.8 (adjust by HCl)

30 µl of protein samples of the same concentration dissolved in mRIPA buffer were mixed with 10 µl 4x Laemmli sample buffer and heated at 95°C for 10 minutes. After cooling, samples were gently loaded onto the gel. In the meantime, 5 µl of WesternC Blotting Standard was loaded onto the sidetrack as the protein size ladder. The electrophoresis cassette ran in Tris/Glycine/SDS running buffer at 150 V for 90 minutes.

3.13.4 Protein transfer

After electrophoresis, proteins were transferred from the gel onto Nitrocellulose (NC) membrane. The filter paper, gel, and NC membrane were soaked in 1x transfer buffer (see below). In the transfer cassette, the NC membrane was in direct contact with the gel, flanked by three filter papers and oriented from the positive to the negative pole. The transfer was performed at 25 V and 1.0 A for 30 minutes. Successful transfer was confirmed by staining of the membrane for protein bands using a Ponceau S solution.

10x Transfer buffer

Tris base	30.3 g
Glycine	144.0 g
Distilled water	up to 1 L

1x Transfer buffer (20% Methanol)

10x Transfer buffer	100 ml
Methanol	200 ml
Distilled water	up to 1 L

3.13.5 Antibody incubation

NC membranes were washed in 1x Tris-buffered saline with Tween20 (TBST) (ingredients are below) and blocked with 5% milk diluted in 1x TBST for 1 hour at room temperature. After 3x washes with 1x TBST, membranes were incubated with a primary antibody at a concentration of 1:500 to 1:4,000 diluted in 1x TBST containing 5% milk for at least 12 hours at 4°C. Membranes were then washed three times in 1x TBST. Incubation of membranes with a secondary antibody was performed at a concentration of 1:10,000 in 1x TBST containing 5% milk. Precision Protein Strep Tactin-HRP Conjugate was also added to the solution of secondary antibody incubation solution at a concentration of 1:5000 for the purpose of developing the protein size ladder. Secondary antibody incubation lasted for 1 hour at room temperature.

10x Tris-buffered saline (TBS)

Tris Base	12 g
Sodium Chloride (NaCl)	87.6g
Distilled water	up to 1L
Adjust pH to 7.6	

Tris-buffered saline with Tween20 (TBST)

1x TBS	1 L
Tween20	1 ml

3.13.6 Chemiluminescence imaging

The developing solution Clarity Western ECL Substrate or Supersignal West Femto Maximum Sensitivity Substrate was used for chemiluminescence imaging. Reagents were mixed at a certain ratio only before imaging. The chemiluminescence imaging was performed using the imager (Bio-Rad). In the imaging cabinet, membranes were exposed for 2 to 300 seconds, depending on the signal intensity. Analysis and normalization relative to the corresponding loading control were performed using the Image Lab 6.1 software.

3.14 RNA sequencing

3.14.1 Target specific reverse transcription

To obtain cDNA of the specific fragment from total RNA, a target-specific reverse transcription was performed using the SuperScript™ IV One-Step system with the ezDNase™ Enzyme kit, which is a combined kit. Because RNA obtained using the Trizol method may contain residual genomic DNA (gDNA), which can form double-strands during reverse transcription and may disturb subsequent sequencing analyses. Thus, gDNA was destructed prior to reverse transcription. The gDNA digestion mix provided by the kit had the following composition.

gDNA digestion mix (4 µl)

10X ezDNase™ buffer	0.4 µl
10X ezDNase™ enzyme	0.4 µl
RNA samples	3.2 µl

gDNA was excluded after incubation at 37°C for 5 minutes. gDNA-free RNA samples were then subject to reverse transcription. The composition of the reaction mix is listed below.

Reverse transcription mix (20 µl)

Template RNA (gDNA-free)	4 µl
2x Platium™ Master Mix	10 µl
Forward primer (10µM)	1 µl
Reverse primer (10µM)	1 µl
SuperScript™ IV RT Mix	0.2 µl
Nuclease-free water	3.8 µl

Target-specific reverse transcription was performed in Thermocycler (Bio-Rad). The following cycle program was used.

Step	Temperature	Time
1	50°C	10 min
2	98°C	2 min
3	98°C	10 s
4	65°C	10 s
5	72°C	30 s
Go to step 3, 35x		
6	72°C	5 min

3.14.2 Transcript purification

The purpose of this part is to purify the cDNA obtained above and clarify that it is reverse transcribed from targeting fragment. Using the method of agarose gel electrophoresis, cDNA can be separated by size. Each gel contains 2% agarose in 1x TAE buffer with 4 μ l/100 ml Midori Green. Ingredients of TAE buffer are indicated below.

50x Tris Acetic Acid EDTA (TAE) buffer

Tris base	2 M
Acetic acid	1 M
EDTA disodium salt dihydrate	50 mM
Distilled water	Up to 1 L

1x Tris Acetic Acid EDTA (TAE) buffer

50x TAE dissolved in distilled water

15 μ l cDNA mixed with 6x TriTrack loading buffer was loaded into each well. Gene ruler 5 μ l was also loaded as the size ladder. The agarose gel electrophoresis lasted for 30 min at a constant 150V.

After electrophoresis, cDNA, as well as the size ladder, could be visualized on the UV table (Thermo Scientific). The clear band with the right size was cDNA derived from the targeting fragment. The gel cube containing the purified cDNA was excised and transferred into a tube. In the next step, cDNA was extracted using the QIAquick Gel extraction kit (QIAGEN) according to the instructions provided by the manufacturer.

3.14.3 Sanger sequencing

Sanger sequencing was performed by an external vendor (Microsynth Seqlab). The pre-mixed samples consisted of 12 μ l cDNA and 3 μ l sequencing oligonucleotide (10 μ M). Sequencing results were analyzed using Chromas 2.6.6.

3.15 Statistical analysis

Independent experiments were repeated at least three times. In each experiment, technical duplicates were included if not specified otherwise. Images or graphs of representative replicates are shown. Error bars indicate \pm standard error of the mean (SEM). To determine statistically significant differences, two-tailed student's T-test for unpaired samples with equal variances and non-parametric ANOVA test were applied. Significance was reached when P-value is below 0.05.

4. Results

4.1 ADAR2 expression is increased during osteoblast differentiation

An unbiased RNA sequencing analysis conducted by former members of the laboratory compared gene expression profiles in aged human bone samples of relatively higher bone mass with samples of relatively lower bone mass. The results indicated that the RNA editing gene adenosine deaminase on double-strand RNA (dsRNA) 2 (ADAR2) could be an epigenetic regulator of human bone mass. Since the samples comprised whole bone and because aged human bone samples contain a high abundance of fat, molecular signals detected in these samples could be derived from osteoblasts or adipocytes. Based on this hypothesis, it is the goal of this thesis to determine the implication of ADAR2 in osteoblast- and/or adipocyte differentiation *in vitro*.

In this study, we performed experiments using the cell line “telomerase reverse transcriptase transduced human mesenchymal stem cell (hMSC-TERT)”. This cell line is derived from human bone marrow. It is well established that these cells can differentiate into both osteoblasts and adipocytes *in vitro*, depending on the type of stimulation¹³⁰. To confirm the ability of hMSC-TERTs to differentiate into osteoblasts, the activity of alkaline phosphatase (ALP), an enzyme secreted by osteoblasts, was determined by staining on day 14 and 21. In addition, mineralization of the extracellular matrix was confirmed by Alizarin red staining on day 21 and 28. Results showed that ALP activity was detectable on day 14 and became more intense on day 21. Alizarin red staining was rather weak on day 21 but strongly detectable on day 28 (Fig. 4.1.A). These findings are consistent with the results on osteoblast differentiation reported by Rauch and colleagues¹³⁰. Quantification of RUNX2 and OCN mRNA expression, two well-established marker genes of osteoblast differentiation, revealed a profound increase in expression as early as day 7. During the subsequent time points, the expression of both genes remained elevated, indicating an ongoing osteoblast differentiation process (Fig. 4.1.B). The increased expression of both genes further confirmed the reliability of the assays and the ability of hMSC-TERTs to adopt an osteoblast phenotype.

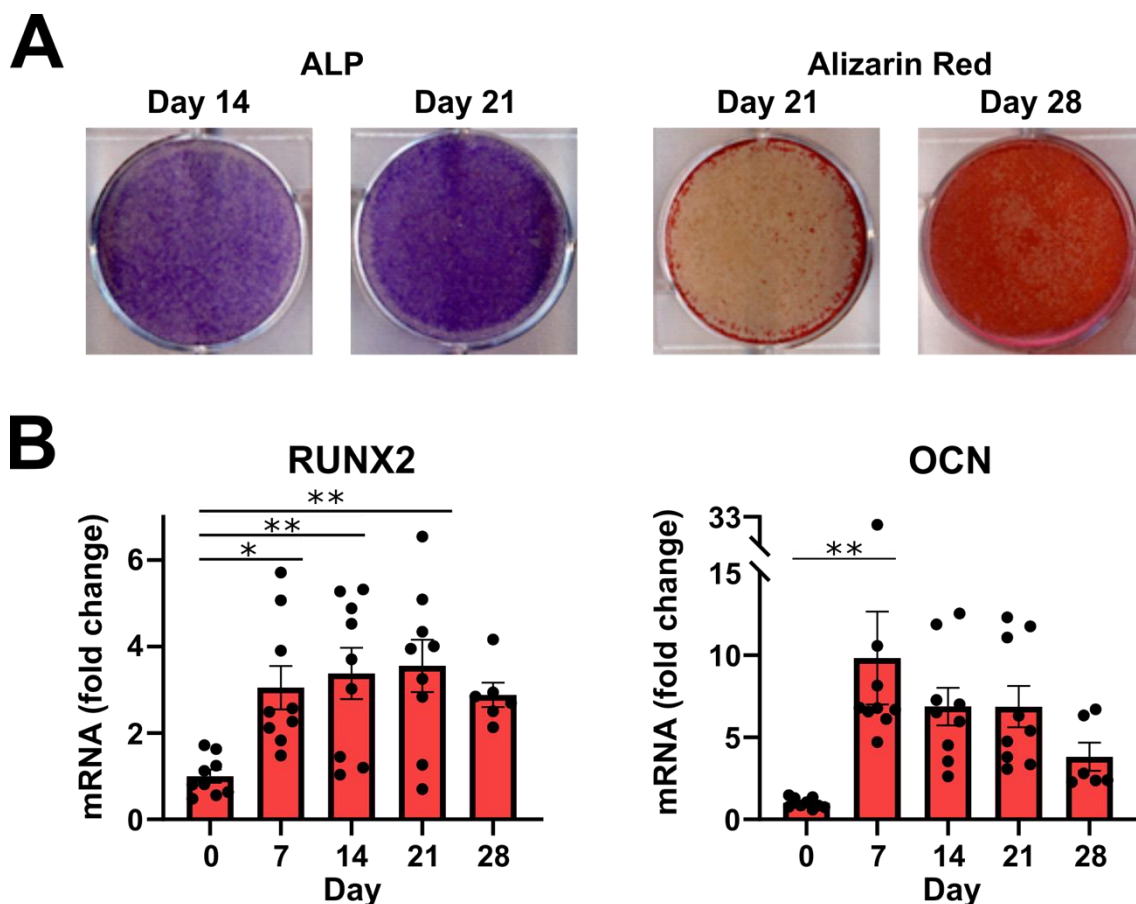


Figure 4.1. hMSC-TERTs differentiate into osteoblasts. **A** Representative image of ALP staining on day 14 and 21; of Alizarin Red staining on day 21 and 28. **B** qPCR analysis of RUNX2 and OCN mRNA expression at different time points during osteoblast differentiation (day 0, 7, 14, 21, and 28). Data are expressed as fold change relative to the average at day 0. Shown are mean values \pm SEM. Statistical significance was determined by one-way ANOVA following Tukey's test. * $p \leq 0.05$, ** $p \leq 0.01$.

Expression of ADAR2 was quantified during osteoblast differentiation. qPCR and immunoblot analysis indicated that the expression of ADAR2 was greatly increased by day 7 and that it remained highly expressed during the remaining course of the experiment (Fig. 4.2). That provides the potential of ADAR2 in the regulation of osteoblast differentiation. Since ADAR1, another family gene, is known to also mediate deamination in physiological conditions, we quantified the expression of ADAR1. The result demonstrated that expression of ADAR1 also increased from day 7 onwards (Fig. 4.2.A). This finding implied that ADAR1 may impact osteoblast differentiation together with ADAR2.

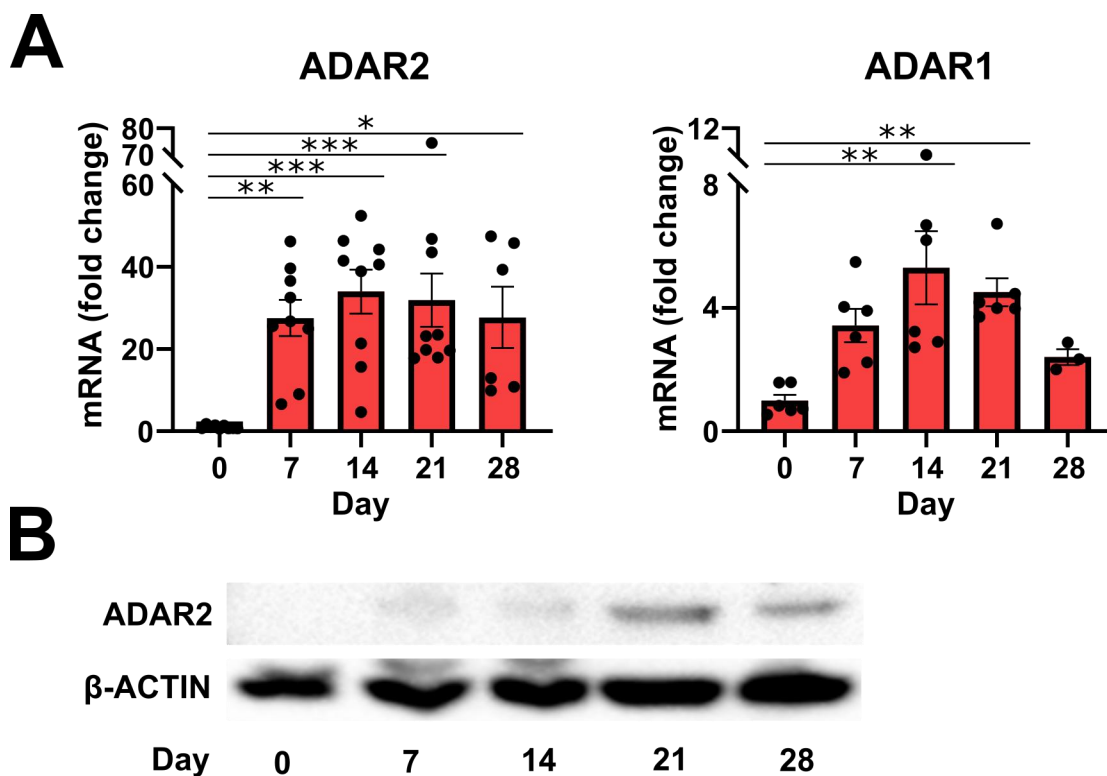


Figure 4.2. ADAR2 mRNA expression is increased during osteoblast differentiation. **A** qPCR analysis of ADAR2 and ADAR1 mRNA expression at different time points during osteoblast differentiation (day 0, 7, 14, 21, and 28). Data are expressed as fold change relative to the average at day 0. Shown are mean values \pm SEM. Statistical significance was determined by One-way ANOVA following Tukey's test. * $p \leq 0.05$, ** $p \leq 0.01$, *** $p \leq 0.001$. **B** Immunoblot analysis of ADAR2 protein expression during osteoblast differentiation, immunoblot for β -Actin was used as the loading control.

4.2 Inhibition of ADAR2 expression does not affect osteoblast differentiation

The increase of ADAR2 expression during osteoblast differentiation suggested that ADAR2 might play a critical role in this process. To determine if ADAR2 indeed affects osteoblast differentiation, ADAR2 expression was inhibited by ADAR2-targeting siRNA (siADAR2). Scrambled siRNA (scr) served as control. To ensure a sufficient siRNA concentration and continuous gene silencing during osteoblast differentiation which lasts for 28 days, transfection was performed twice; 1 day prior to stimulation (day -1) and 14 days after stimulation (day 14). qPCR analysis revealed that under these conditions, ADAR2 expression remained suppressed compared to scr-treated control cells during osteoblast differentiation (Fig. 4.3). A concomitant increase of ADAR1 expression by ADAR2-targeting siRNA as part of a potential compensatory mechanism was excluded (Fig. 4.3).

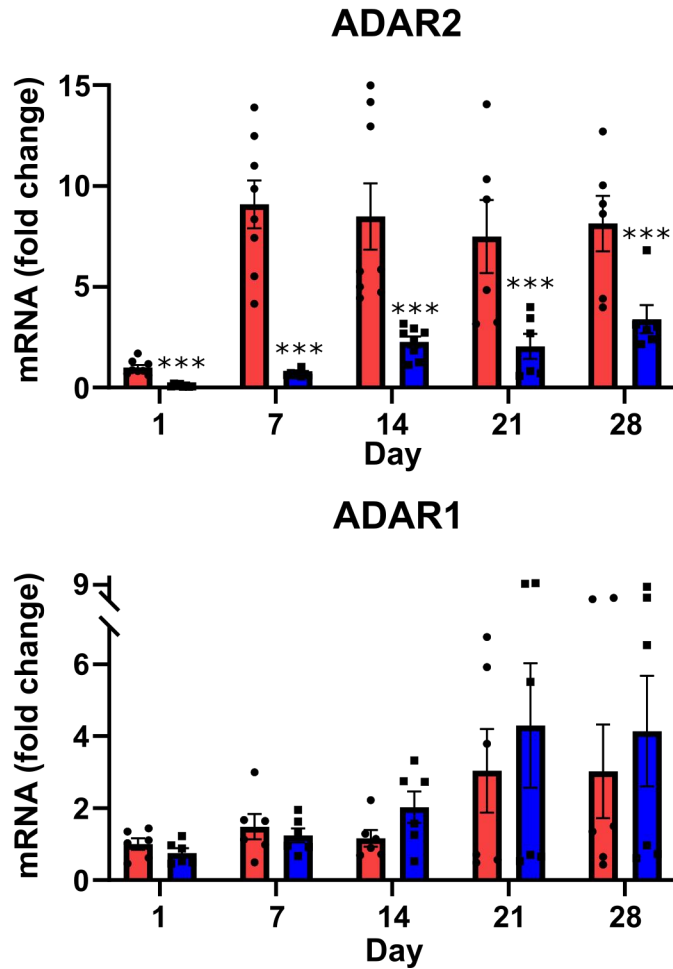


Figure 4.3. Transient siRNA transfection decreases ADAR2 expression without affecting ADAR1 expression during osteoblast differentiation. qPCR analysis of ADAR1 and ADAR2 mRNA expression in hMSC-TERTs upon transient transfection with scrambled (scr) control (red bar) or siADAR2 (blue bar) during osteoblast differentiation. Presented are fold changes normalized to the average of scr at day 1. Shown are mean values \pm SEM. Statistical analysis was performed by student t-test comparing siADAR2 or siADAR1 vs. scr for each time point. *** $p \leq 0.001$.

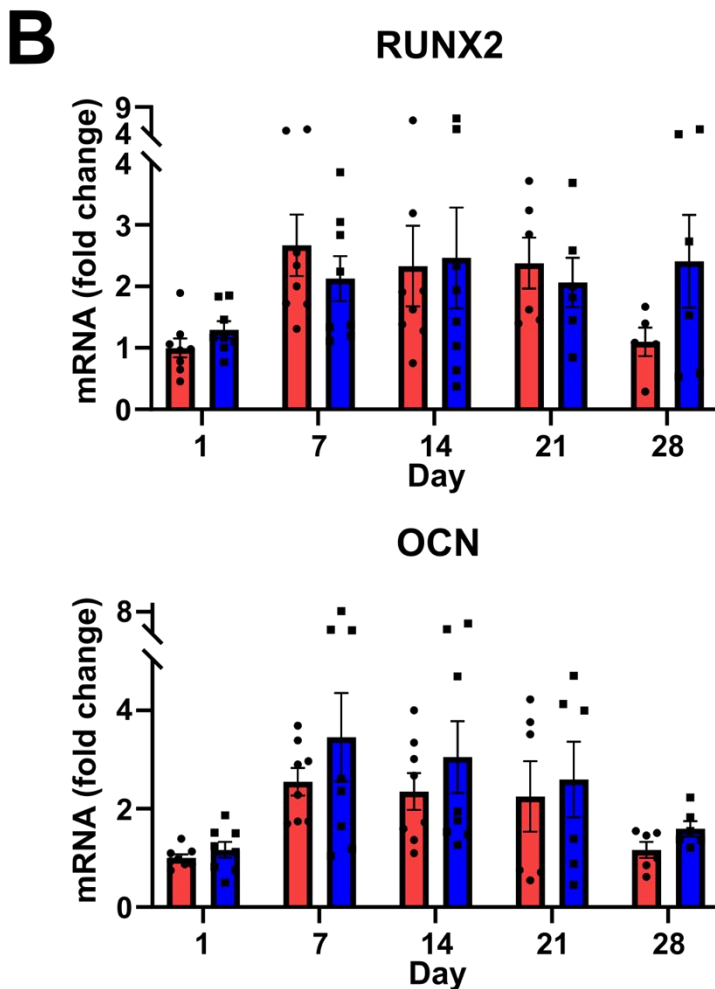
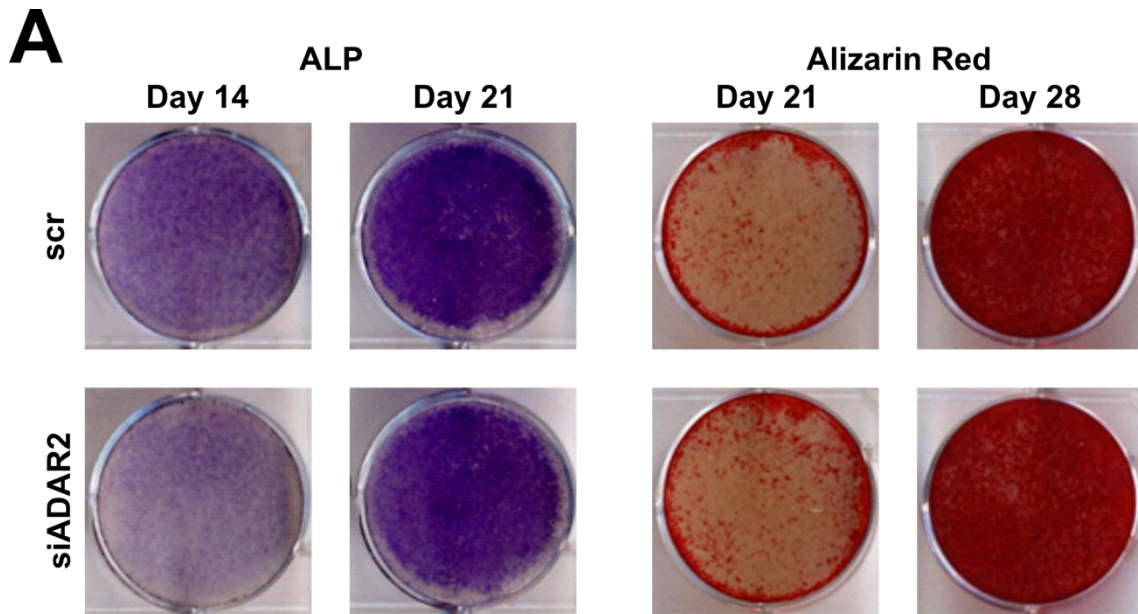


Figure 4.4. Inhibition of ADAR2 expression does not affect osteoblast differentiation. **A** Representative image of ALP staining of hMSC-TERTs upon transient transfection with scrambled (scr) control siRNA (upper row) or siADAR2 (lower row) by day 14 and 21. Representative image of Alizarin red staining of cells cultured under the same conditions was performed by day 21 and 28. **B** qPCR analysis of RUNX2 and OCN mRNA expression under the same experimental condition as in A. Presented are fold changes compared to scr at day 1. Shown are mean values \pm SEM. Statistical analysis was performed using student t-test, comparing siADAR2 vs. scr for each time point.

ALP staining revealed no difference between both groups by day 14 and 21 (Fig. 4.4.A). In addition, Alizarin Red staining on day 21 and 28 did also not show any difference in late-stage mineralization between siADAR2 and scr (Fig. 4.4.A). Furthermore, the qPCR analysis revealed that inhibition of ADAR2 did not alter the expression of RUNX2 or OCN (Fig. 4.4.B). These findings support the conclusion that inhibition of ADAR2 does not affect osteoblast differentiation.

4.3 ADAR2 expression is increased during adipocyte differentiation

In the context of elucidating the role of ADAR2 in adipocyte differentiation, hMSC-TERTs were stimulated to differentiate into adipocytes. After 21 days of stimulation, lipid droplets accumulated intracellularly and were visualized by oil red O staining (Fig. 4.5.A). Expression of PPAR γ mRNA, a key transcription factor of adipocyte differentiation, was increased during this process, indicating a successful adipocyte differentiation. Consistently, expression of the adipocyte-related genes FABP4 and ADIPOQ was detectable by day 14 with a further increase by day 21 (Fig. 4.5.B). qPCR results combined with staining results proved the reliability of the assay and the ability of hMSC-TERTs to differentiate into adipocytes. Furthermore, findings are consistent with the results reported by Rauch et al. who described the versatility of this cell line¹³⁰.

Similar to the findings made during osteoblast differentiation, expression of ADAR2 mRNA was also increased during adipocyte differentiation. Compared to non-stimulated cells by day 0, ADAR2 expression was increased from day 7 onwards at the mRNA and protein level as determined by qPCR and immunoblot blot analysis, respectively (Fig. 4.6). Expression of ADAR1 mRNA demonstrated a trend towards an increase at day 7, 14, and 21 compared to day 0 but did not reach significance (Fig. 4.6.A). These results indicate that ADAR2 but not ADAR1 plays a role during adipocyte differentiation.

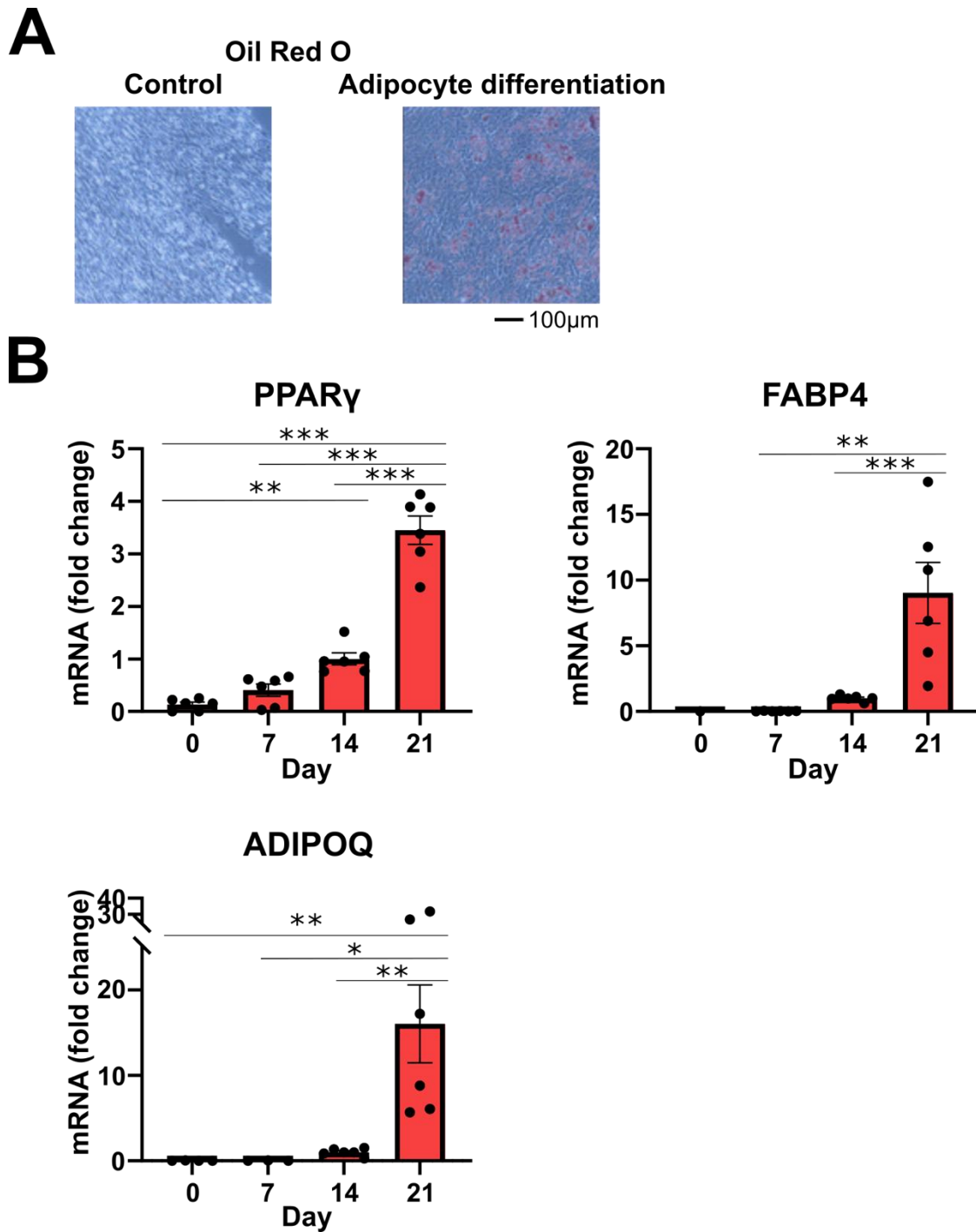


Figure 4.5. hMSC-TERTs differentiate into adipocytes. **A** Representative microscope image of oil red O-stained hMSC-TERTs upon adipocyte differentiation at day 21 compared to control cells with no stimulation (10x). **B** qPCR analysis of PPAR γ , FABP4, and ADIPOQ mRNA expression at different time points during adipocyte differentiation (day 0, 7, 14, and 21). Data are expressed as fold change relative to the average at day 14. Shown are mean values \pm SEM. Statistical significance was determined by one-way ANOVA following Tukey's test. * $p \leq 0.05$, ** $p \leq 0.01$, *** $p \leq 0.001$.

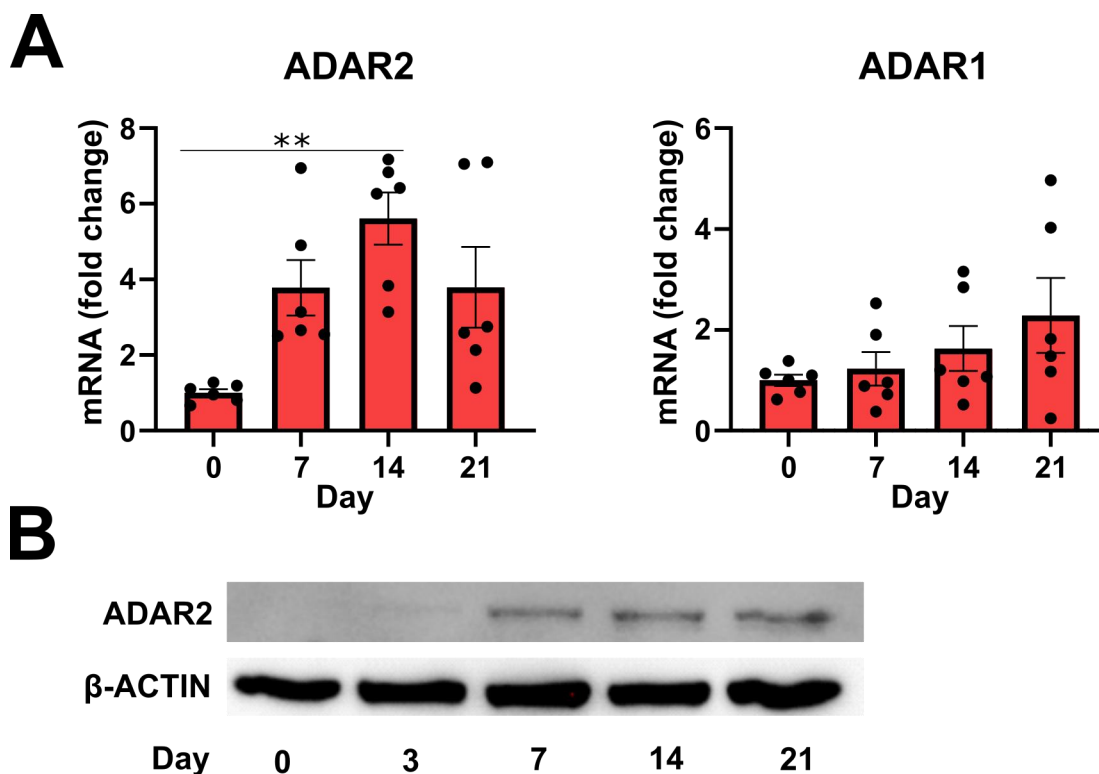


Figure 4.6. ADAR2 mRNA expression increases during adipocyte differentiation. **A** qPCR analysis of ADAR2 and ADAR1 mRNA expression at different time points during adipocyte differentiation (day 0, 7, 14, and 21). Data are expressed as fold change compared to the average at day 0. Shown are mean \pm SEM. Statistical significance was determined by One-way ANOVA following Tukey's test. $**p \leq 0.01$. **B** Immunoblot analysis of ADAR2 protein expression during adipocyte differentiation. Immunoblot for β -Actin was used as loading control.

4.4 Inhibition of ADAR2 expression decreases adipocyte differentiation

To investigate the role of ADAR2 during adipocyte differentiation, ADAR2 expression was inhibited by transient transfection of ADAR2-targeting siRNA (siADAR2). Scrambled (scr) siRNA served as control. To ensure continuous gene silencing throughout the course of adipocyte differentiation for 21 days, transient transfection was performed twice during the differentiation process; 1 day prior to stimulation (day -1) and 10 days after stimulation (day 10). qPCR analysis confirmed that ADAR2 expression was indeed suppressed by siADAR2 during the entire period of adipocyte differentiation (Fig. 4.7). Consistent with the previous findings, ADAR1 mRNA expression was not increased in a compensatory manner (Fig. 4.7).

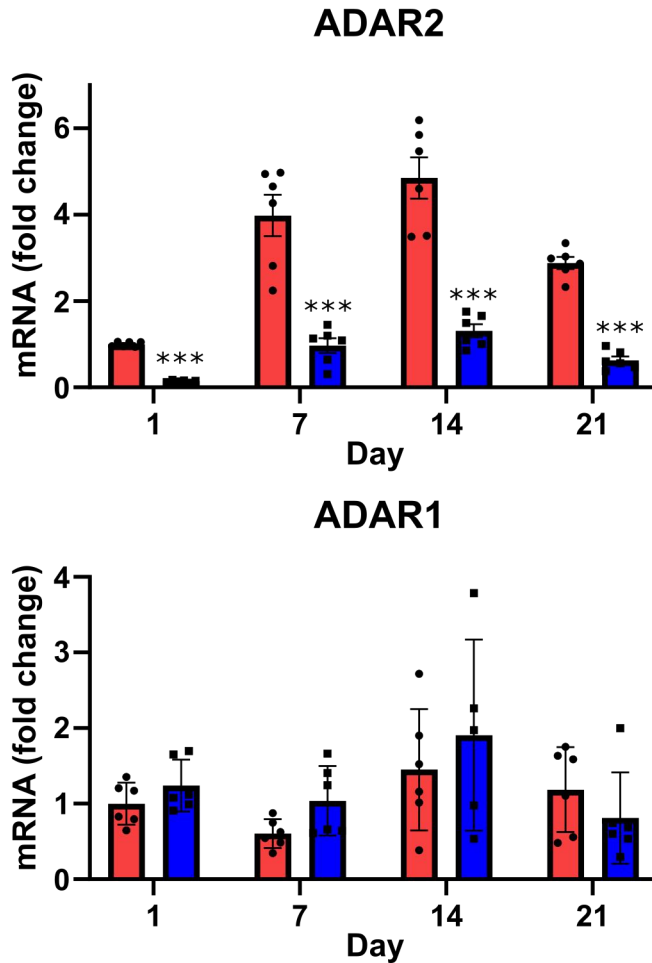


Figure 4.7. Inhibition of ADAR2 expression does not affect the abundance of ADAR1 mRNA during adipocyte differentiation. qPCR analysis of ADAR2 and ADAR1 mRNA expression hMSC-TERTs upon transient transfection with scrambled (scr) control (red bar) siRNA or siRNA targeting ADAR2 (siADAR2, blue bar) during adipocyte differentiation. Presented are fold changes compared to the average of scr at day 1. Shown are mean \pm SEM. Statistical significance was determined by student t-test comparing siADAR2 vs. scr at each time point. *** $p \leq 0.001$.

Lipid droplets became visible from day 17 onwards. Merged low magnification images of oil red O-stained cell layers revealed no difference in differentiation by day 17 (Fig. 4.8.A). However, during later stages of adipocyte differentiation (day 21), oil red O staining demonstrated an impaired adipocyte differentiation of cells in which the expression of endogenous ADAR2 was antagonized (Fig. 4.8.A). Because lipid droplets are visualized by oil red O staining and are fluorescent, their abundance was quantified using fluorescent imaging. Quantification revealed that by day 21, the abundance of lipid droplets in the siADAR2-treated group was significantly reduced compared to the control group (Fig. 4.8.B).

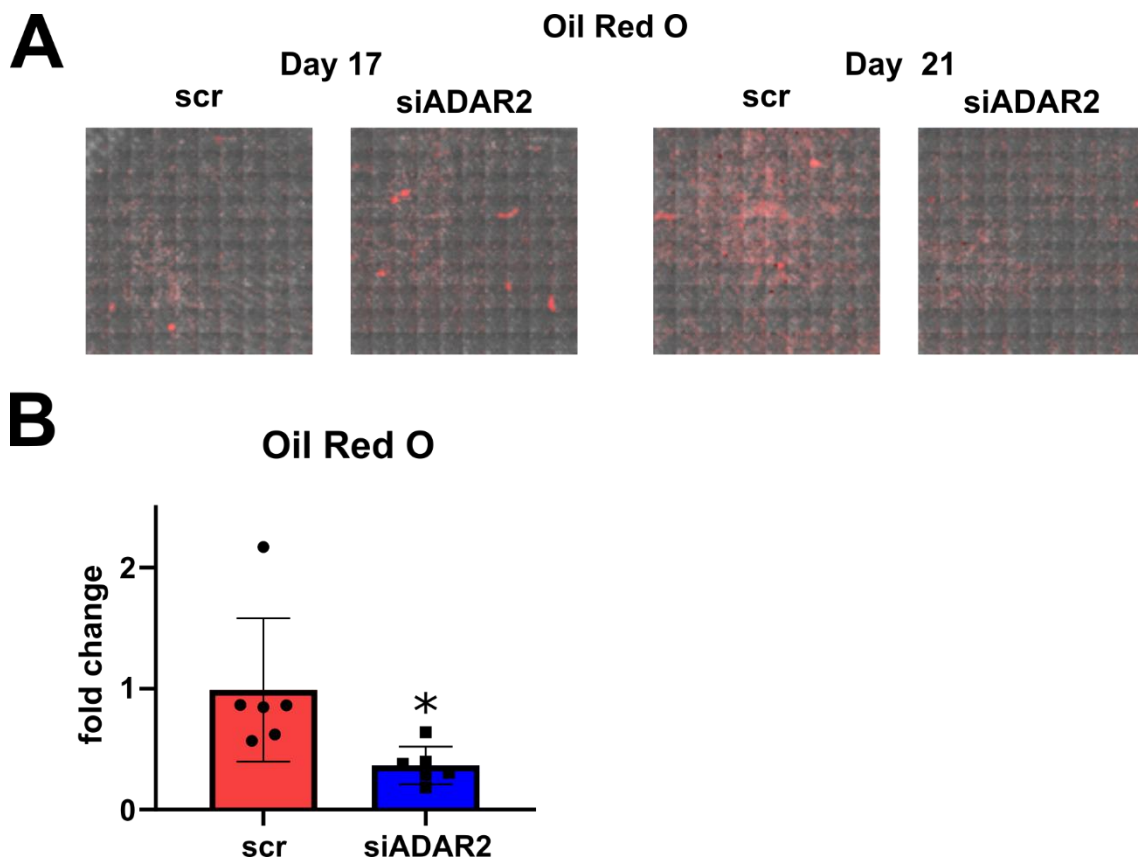


Figure 4.8. Inhibition of ADAR2 expression impairs late-stage adipocyte differentiation. A Representative merged images of oil red O staining at day 17 and 21 in cells in which expression of endogenous ADAR2 was antagonized (siADAR2) compared to scrambled (scr) control. **B** Quantification of oil red O staining at day 21. Data are expressed as fold changes compared to the average of scr at day 21. Shown are mean values \pm SEM. Statistical significance was determined by student t-test. * $p \leq 0.05$.

In addition, qPCR analysis revealed that siADAR2 transfection mildly promotes adipocyte differentiation at early stages. In siADAR2-treated cells, expression of FABP4 and ADIPOQ was suppressed at day 14. Expression of PPAR γ was reduced at both, day 7 and 14 (Fig. 4.9). However, at a late stage (day 21), qPCR analysis revealed consistency with the results obtained by oil red O staining. Briefly, expression of the adipocyte-related genes FABP4 and ADIPOQ was lower in the siADAR2-treated group compared to scr control at day 21 (Fig. 4.9). Interestingly, expression of the master transcription factor of adipogenesis PPAR γ was not significantly altered by siADAR2 (Fig. 4.9). These results indicate that despite a mild increase at an early stage, ADAR2 inhibition decreased adipocyte differentiation at a later differentiation stage and in a rather PPAR γ expression-independent manner.

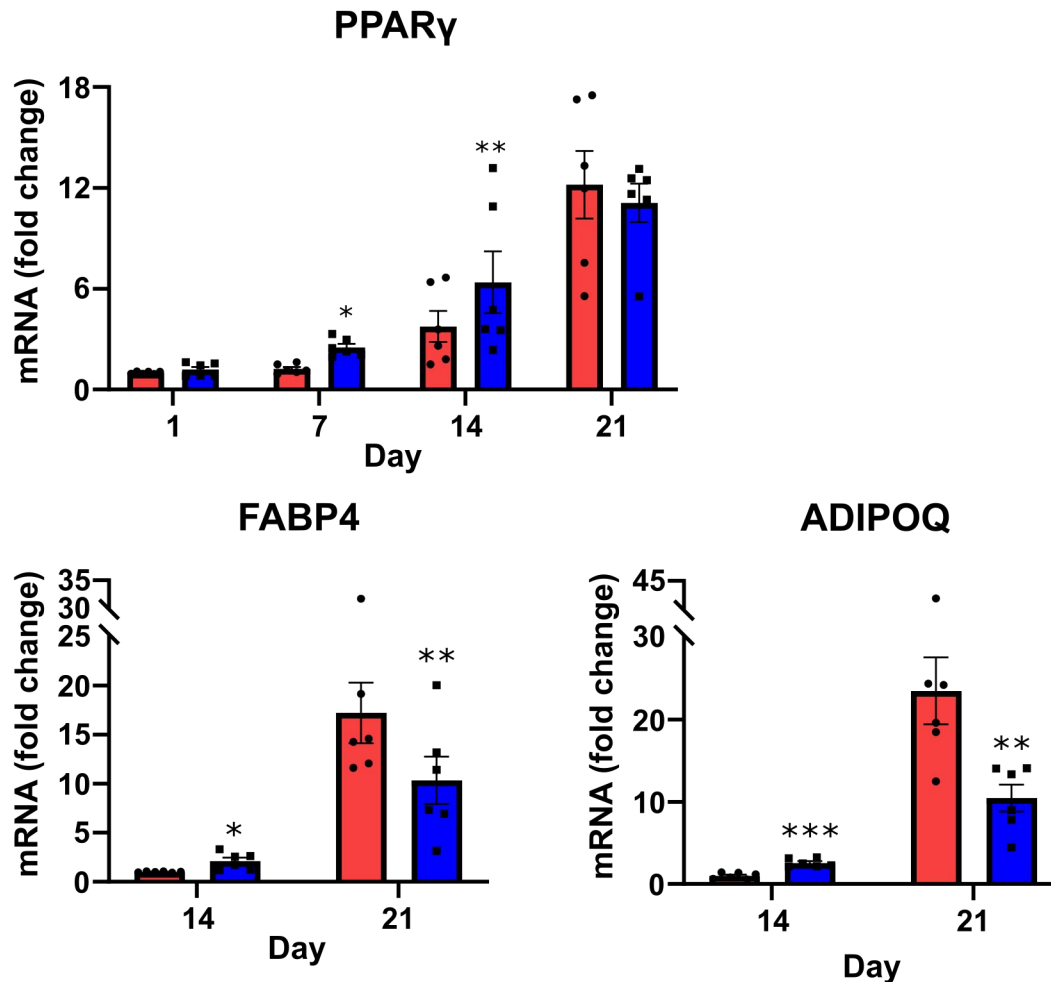


Figure 4.9. Inhibition of endogenous ADAR2 mRNA expression attenuates late-stage adipocyte differentiation. qPCR analysis of PPAR γ , FABP4, and ADIPOQ mRNA expression in hMSC-TERTs upon transient transfection with scrambled (scr) control (red bar) or siADAR2 (blue bar) during adipocyte differentiation. Presented are fold changes compared to the average of scr at day 1 (PPAR γ) or at day 14 (FABP4 and ADIPOQ). Shown are mean values \pm SEM. Statistical significance was determined by student t-test comparing siADAR2 vs. scr at each time point. * $p \leq 0.05$, ** $p \leq 0.01$.

4.5 Inhibition of ADAR2 expression impairs editing of GRIA2 during adipocyte differentiation

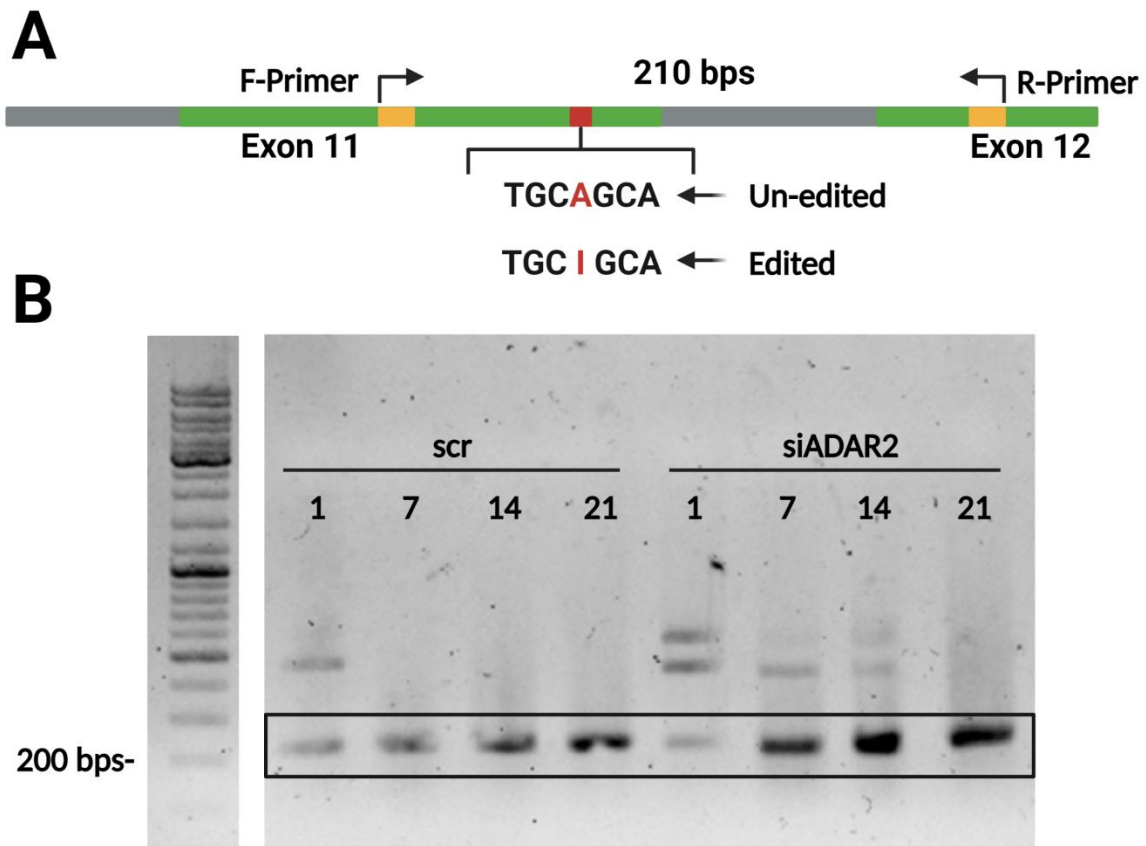
The results presented thus far demonstrate that transient transfection of siADAR2 suppresses the RNA expression of ADAR2 in differentiating hMSC-TERTs. This raised questions about the functional relevance of this observation.

The predominant function of ADAR2 is RNA editing as a component of post-transcriptional modification. The post-transcriptional modification comprises processes occurring at the RNA level, by which the primary transcript undergoes a modification and maturation process. Specifically, ADAR2 recognizes and interacts with dsRNA structures and mediates deamination, thereby converting adenosine (A)

into inosine (I) (A-to-I editing). Since inosine pairs preferentially with cytosine (C) which is the same as guanosine (G), A-to-I editing results in a single-nucleotide switch on the sequence of RNA. It subsequently affects downstream processes including RNA generation, localization, degradation, and translation⁹².

In humans, A-to-I editing events are abundant. In addition to ADAR2, also ADAR1 has been proven to bear enzyme activity and many A-to-I editing events are mediated by both ADAR1 and ADAR2¹³². Among these editing events, A-to-I editing of the gene encoding glutamate ionotropic receptor AMPA type subunit 2 (GRIA2) has been proven to be specifically mediated by ADAR2 but not ADAR1¹⁰⁰. This editing event occurs in exon 11 of the GRIA2 gene. As a result, the amino acid sequence becomes altered from Glutamine (Q) to Arginine (R). Hence, this ADAR2-specific A-to-I editing site is commonly named GRIA2 Q/R site^{107,133}.

Therefore, we aimed to investigate the functional implication of ADAR2 by determining the editing efficiency at the GRIA2 Q/R site using Sanger sequencing. Since the Q/R site is located at the 3' end in exon 11, two oligonucleotides were designed that anneal within exons 11 and 12 and therefore flank the site of editing. The oligonucleotides span a length of 210 base pairs without any intron in between (Fig. 4.10.A). After gDNA elimination, total RNA was reverse transcribed using GRIA2 Q/R site-specific oligonucleotides. Using the method of agarose gel electrophoresis, cDNA was separated by size and only cDNA of a length of 210 base pairs was derived from the GRIA2 Q/R site contained fragment (Fig. 4.10.B). Then, purified cDNA was isolated from the agarose gel and performed Sanger sequencing.



Created with Bio-Rednder.com

Figure 4.10. Obtaining transcripts of the GRIA2 Q/R site. **A** The Q/R site is located at the 3' end in exon 11 of GRIA2. Under physiological conditions, ADAR2 mediated A-to-I editing alters the sequence from CAG into CIG. Two oligonucleotides were designed as forward (F) and reverse (R) primers for reverse transcription of the GRIA2 Q/R site. Exon: green bar, Intron: grey bar, Designed oligonucleotide: yellow bar, Q/R site: red bar. **B** After reverse transcription, bands of 210 bps (rectangle) were excised from the agarose gel, purified, and subjected to Sanger sequencing.

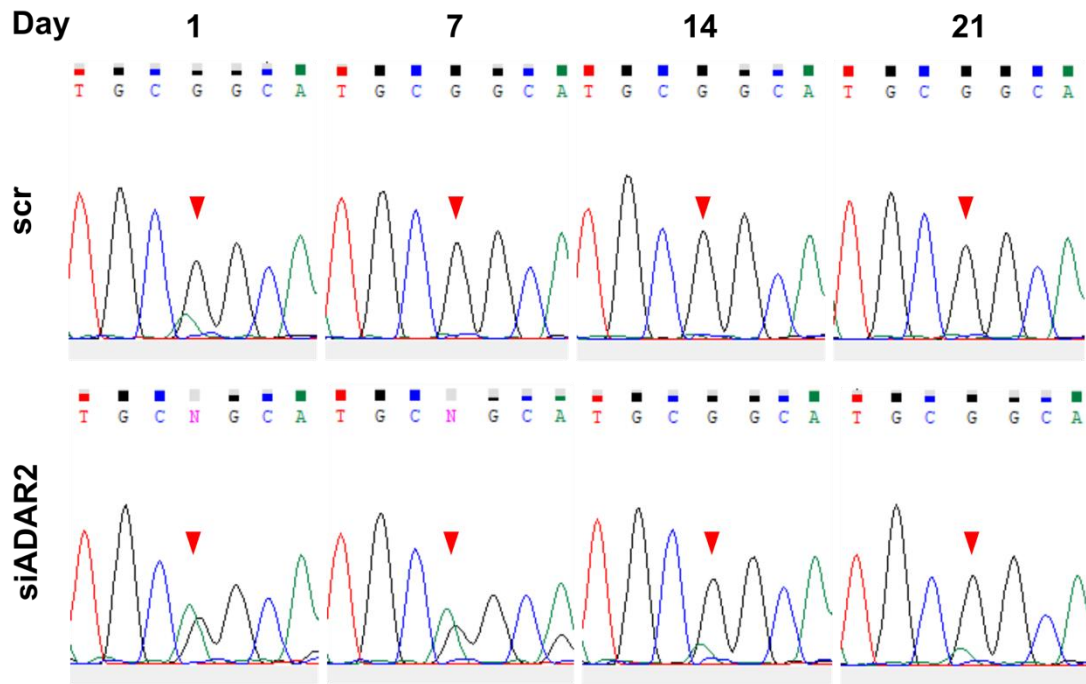


Figure 4.11. Inhibition of ADAR2 impairs A-to-I editing at the Q/R site of GRIA2 mRNA. Sanger sequencing chromatograms of the GRIA2 Q/R site at differentiation day 1, 7, 14, and 21 upon transfection of adipocytes with scrambled (scr) control or siADAR2. In scr-treated cells, the GRIA2 Q/R site was partially edited on day 1 and became fully edited by day 7. Cells treated with siADAR2 demonstrated an incomplete editing of this site throughout the course of differentiation. Sequencing chromatograms were visualized using Chromas. The red triangles indicate the altered absorbance peaks at the GRIA2 Q/R site. Curved lines indicate the absorbance peaks of individual nucleotides: green represents adenosine (A), red represents thymine (T), blue represents cytosine (C), and black represents guanine (G). Inosine is recognized as G. Letters depicted on the top are nucleotides identified automatically by Chromas. N means non-identified, which indicates no-nucleotide is dominant enough to identify. Rectangles above letters indicate the possibility of identification.

In this study, Sanger sequencing was outsourced to the company Microsynth Seqlab. Chromatograms were visualized using the software Chromas 2.6.6. After reverse-transcription, inosine generated by ADAR2 at the GRIA2 Q/R site was illustrated as guanine (G). The sequencing results demonstrate that at day 1 the GRIA2 Q/R site was only partially edited regardless of whether adipocytes were transfected with scr or siADAR2 oligonucleotides. However, as adipocyte differentiation continued, this site became fully edited in scr-treated control cells while in adipocytes treated with siADAR2 the GRIA2 Q/R site remained unedited. These results suggested that the inhibition of ADAR2 caused the PPAR γ expression-independent deficit of adipocyte differentiation by decreasing the editing event on the GRIA2 Q/R site.

5. Discussion

Mesenchymal stem cells (MSCs) are multipotent stromal cells residing in the bone marrow that bear the potential to differentiate into osteoblasts or adipocytes^{3,81,82}. The molecular mechanisms governing the differentiation of MSCs towards the osteoblast lineage or into adipocytes are tightly regulated^{134,135}. This thesis provides a contribution to this field by describing a potential epigenetic mechanism mediated by adenosine deaminase on double-strand RNA 2 (ADAR2) affecting adipocyte differentiation of MSCs.

ADAR2, as well as its family members, is known to mediate adenosine to inosine (A-to-I) editing, an evolutionarily conserved mode of RNA modification that occurs in virtually all cell types. Since inosine base pairs with cytidine, A-to-I editing causes RNA sequence alterations, which can affect biological processes like RNA biogenesis, RNA interference, and protein generation and functions⁹². ADAR2 related A-to-I editing is deeply investigated in the brain and central nervous system. A canonical editing event occurs on the exon of GRIA2, which converts the amino acid from glutamine (Q) into arginine (R). In physiological, the GRIA2 Q/R site is completely edited and solely performed by ADAR2¹⁰⁷. This editing is critical in the central nervous system since mice with un-edited GRIA2 Q/R site caused by germline deletion of ADAR2 suffered severe seizures and die young¹⁰⁸. However, how ADAR2 behaves in other tissues is less known.

In this study, ADAR2 expression was found to be increased in the early stage of both osteoblast and adipocyte differentiation. To determine the functional relevance of this observation, ADAR2 expression was inhibited transiently during differentiation towards either lineage. As a result, osteoblast differentiation remained unaffected by ADAR2 inhibition demonstrated by unchanged phenotypic staining and an unaltered expression of osteoblast-related genes such as RUNX2 and OCN. In contrast, adipocyte differentiation was markedly impaired at the later stage by ADAR2 inhibition as confirmed by a weaker staining for lipid droplets and a decreased expression of adipocyte-related genes including FABP4 and ADIPOQ. However, the expression of PPAR γ , the master transcriptional regulator of adipocyte differentiation¹³⁶, was unchanged, suggesting that the underlying mechanism might be mediated via decreasing PPAR γ transcriptional activity rather than affecting its expression. By sequencing, ADAR2 inhibition decreased the editing efficiency on the

GRIA2 Q/R site. These findings demonstrate that GRIA2 is a ADAR2 editing site that might affect adipocyte differentiation.

Potential roles of ADAR2 in MSCs differentiations were proposed since one of the ongoing research projects in the laboratory observed a higher expression of ADAR2 in human bone samples with lower density compared to samples with higher bone density. This study revealed that ADAR2 expression is relatively low in early stage, not yet differentiated MSCs but greatly increased during osteoblast and adipocyte differentiation. This strongly suggested that ADAR2 is involved in the differentiation of both lineages. Expression of ADAR2 is regulated by the transcriptional factor cAMP response element-binding protein (CREB). Peng et al. observed that ADAR2 expression and consecutively editing efficiency of ADAR2-mediated events were both deficits in CA1 pyramidal neurons of rats with forebrain ischemia. Moreover, the reduced ADAR2 expression and function were recovered by constitutive activation of CREB¹³⁷. This is of relevance to this study since CREB plays an important role in the differentiation and function of MSCs and their descendants. In particular, CREB is an important transcriptional factor for the crosstalk between PTH- and BMP signaling in osteoblasts¹³⁸. In addition, CREB induces the expression of C/EBP β , an early stage transcription factor of adipocyte differentiation¹³⁹.

Based on the observation that ADAR2 expression increases during the differentiation of early-stage MSCs into osteoblasts, the hypothesis arose that ADAR2 is functionally relevant for osteoblast differentiation. To test this hypothesis, the increase in ADAR2 expression was prevented by transiently transfecting MSCs with ADAR2-targeting siRNA. The results revealed that compared to MSCs transfected with scrambled siRNA, attenuation of ADAR2 expression did not affect MSC differentiation into osteoblasts. These findings demonstrate that ADAR2 expression is dispensable for osteoblast differentiation.

Unlike ADAR2, another gene family member ADAR1 was reported as positive regulator of osteoblast differentiation. A study reported by Yu et al. described that mice bearing a postnatal targeted deletion of ADAR1 in bone presented a lower bone density compared to control littermates. Consistently, expression of OCN and osterix in bone tissue were decreased¹⁴⁰. These observations formed the basis on which the authors reached the conclusion that ADAR1 supports the gain in bone density via

osteoblast-dependent mechanisms independent of osteoclast function¹⁴⁰. Accompanying *in vitro* experiments revealed, that ADAR1 supports osteoblast differentiation by increasing the expression of osterix. Furthermore, proliferation of pre-osteoblasts was stimulated by increasing the expression of the cell cycle-related genes cyclin D1 and A1¹⁴⁰. The observation reported by Yu et al. could explain why restricting the expression of ADAR2 does not inhibit osteoblast differentiation. It is possible that ADAR1 alone is sufficient to support osteoblast differentiation or that it compensates for the lack of ADAR2. In this study, we did not detect an increase in ADAR1 expression in the absence of ADAR2. Thus, this potential compensatory mechanism at least does not occur by the abundance of ADAR1.

Nevertheless, this potential compensatory mechanism is possible since many findings support the notion that some editing events are mediated by both ADAR1 and ADAR2. Compared with ADAR2, ADAR1 contains a specific Z-DNA binding domain and more numbers of ds-RNA binding domain⁹⁴, which provides ADAR1 the structural ability to bind to the same substrates as ADAR2. The study of Lehmann et al. demonstrated that ADAR1 had the same editing preference as ADAR2, both rarely target adenosines less than eight nucleotides away from the 3' terminus¹³². Moreover, some studies directly revealed this overlapping editing character. Riedmann et al. reported that editing efficiency on several locations was not completely decreased when only ADAR1 or ADAR2 was deleted¹⁴¹. Another study from Japan used RNA immunoprecipitation-sequencing in Hela cells and reported that transcripts from 39 genes were interacting with both ADAR1 and ADAR2¹⁴².

As next step, we aimed to elucidate whether ADAR2 is functionally relevant for adipocyte differentiation. Interestingly and different from osteoblasts, silencing of ADAR2 expression in MSCs during adipocyte differentiation using siRNA diminished the adipocyte differentiation capacity of MSCs. Compared to MSCs treated with scrambled control siRNA, MSCs transiently transfected with ADAR2-targeting siRNA were impaired in their ability to accumulate lipid droplets over time. These findings demonstrate that ADAR2 is, unlike in osteoblasts, of critical functional relevance for adipocyte differentiation.

Several lines of evidence further support the implication of ADAR2 in adipocyte biology. Singh et al. observed that overexpression of ADAR2 in mice under the control of the human cytomegalovirus promoter resulted in adult-onset obesity. The

obesity phenotype was likely the consequence of behavioral hyperphagia since the obesity phenotype disappeared under conditions of food restriction¹⁴³. Besides hyperphagia, more behavioral abnormalities were reported in subsequent studies including the preference for a high-fat-contained diet¹⁴⁴ and increased depression- and anxiety-related activities¹⁴⁵. The authors attributed these behavioral changes to mis-editing of the serotonin receptor 2C, leading to an increased hypothalamus-pituitary adrenal axis activity^{144,145}. It is noteworthy to mention that mice overexpressing a deaminase-deficient mutant of ADAR2 also presented with an obesity phenotype, suggesting that the increase in weight might be, at least in part, also mediated by editing-independent mechanisms¹⁴³.

In addition to affecting behavior, ADAR2 has also been reported to promote lipid accumulation via the endocrine system. Gan et al. reported that in high-fat diet induced insulin-resistant mice, the expression of ADAR2 was significantly higher in pancreatic β -cell¹⁴⁶. They illustrated that inhibition of ADAR2 impairs the exocytosis of insulin. Specifically, expressions of Munc18-1 and synaptotagmin-7, two important molecules in the process of cell exocytosis, were decreased¹⁴⁷.

These findings together support the notion that ADAR2 is a positive regulator of overall fat accumulation. However, findings reported here demonstrate that ADAR2 promotes fat biogenesis by directly increasing adipocyte differentiation of human MSCs. This is novel and goes beyond of what is known about the role of ADAR2 in the central nervous- and the endocrine system.

To further understand the mechanism by which ADAR2 increases adipogenesis, expression of adipocyte-related genes was quantified in MSCs treated with ADAR2-targeting siRNA. Consistent with the phenotypic observation of a diminished oil red O staining, expression of FABP4 and ADIPOQ was decreased at later stages of adipocyte differentiation. However, it is interesting to note that expression of PPAR γ was not affected by downregulation of ADAR2 expression.

The expression of adipocyte-related genes like FABP4 and ADIPOQ is induced by several transcriptional factors^{64,148}. Specifically, a genome-wide ChIP-sequencing using cells of the 3T3-L1 adipocyte cell line identified binding sites of C/EBP and PPAR γ in the FABP4 promoter¹⁴⁹. Another study examined the promoter sequence of mouse ADIPOQ and identified many putative binding sites for the transcription factors SREBP, C/EBP, and PPAR γ ⁷⁸. However, the traditional notion considers

PPAR γ as the master regulator of adipocyte differentiation. For instance, retroviral overexpression of PPAR γ is sufficient to direct fibroblast differentiation into adipocytes¹⁵⁰. Additionally, PPAR γ is indispensable for adipogenesis since ectopic expression of C/EBP α in PPAR γ ^{-/-} fibroblasts fails to induce adipocyte differentiation¹⁵¹. However, the ability of C/EBP α ^{-/-} cells to become adipocytes was restored upon ectopic expression of PPAR γ ¹⁵². In conclusion, no clear evidence exist that some factors can promote adipocyte differentiation in the absence of PPAR γ . Thus, a possible mechanism might be that inhibition of ADAR2 expression impairs PPAR γ transcriptional activity rather than affecting its expression.

PPAR γ is subject to multiple post-transcriptional modifications known to impair its transcriptional activity. For example, phosphorylation of serine 112^{153,154} or serine 273¹⁵⁵ inhibit PPAR γ activity by decreasing the recruitment of transcriptional co-activators. Small ubiquitin-like modifier (SUMO) 1-related modification of lysine 107 was reported to diminish PPAR γ transcriptional activity¹⁵⁶. However, it demands more experiments to further clarify this potential mechanism.

The results obtained within this project suggest that reduced ADAR2 expression leads to a decrease in adipocyte differentiation. We therefore aimed to investigate how ADAR2-mediated editing events change in response to ADAR2 inhibition. To address this question, we sequenced the GRIA2 Q/R site since it has been reported to be edited specifically by ADAR2¹⁰⁷. Our data reveal that concomitant with a decrease in adipocyte differentiation, the Q/R site of GRIA2 mRNA was only partially edited in the context of ADAR2 inhibition, while site editing occurred to the full extent in the control group. These findings confirm that ADAR2 is indeed functionally relevant for editing of the GRIA2 Q/R site. Since GRIA2 is the important subunit of AMPA inducible glutamate receptor, it is reasonable to hypothesize that the glutamate receptor is implicated in the ADAR2-dependent regulation of adipocyte differentiation. This hypothesis is supported by a study of Horsch et al. demonstrating that ADAR2-deficient mice bearing the edited version of GRIA2 had normal adipose tissue¹⁵⁷.

The glutamate receptor, as the transmembrane protein related to neurotransmitter actions, is considered to be barely expressed outside the nervous system. However, experiments described within this thesis report a low expression of GRIA2 in MSCs during adipocyte differentiation. This novel observation is supported

by another study by Nicolaysen et al. who reported the detection of GRIA2 in both brown- and white adipose tissue in mice using immunofluorescence microscopy¹⁵⁸. Moreover, γ -aminobutyric acid, another neurotransmitter, was reported to exert effects on adipose tissue metabolism¹⁵⁹. These findings support the hypothesis that glutamate receptors influence adipocyte differentiation.

Editing of the GRIA2 Q/R site causes functional changes of the AMPA receptor since it renders the receptor from Ca^{2+} permeable to impermeable¹⁰⁷. In this study, the editing efficiency on GRIA2 was greatly impaired in ADAR2-deficient adipocytes. That means that ADAR2 inhibition retained the AMPA receptor Ca^{2+} permeable, allowing an ongoing Ca^{2+} influx. The Ca^{2+} concentration inside the cell is about 100 nmol/L, which is about 10,000 times lower than outside the cell¹⁶⁰. However, as a ubiquitous second messenger molecule, Ca^{2+} is involved in various cellular events including excitability, exocytosis, motility, apoptosis, and transcription¹⁶¹. Regarding the aspect of adipogenesis, Ca^{2+} is considered as negative factor. Many *in vitro* studies reported that cells treated with a medium of high Ca^{2+} -concentration, which caused an enhanced Ca^{2+} influx, decreased adipocyte differentiation^{162,163}. Moreover, the direct way of increasing intracellular Ca^{2+} concentration using inhibitors of Ca^{2+} -ATPase caused lower expressions of adipocyte-related genes and less lipid accumulation in 3T3-L1 pre-adipocytes^{164,165}.

It is noteworthy that AMPA-inducible glutamate receptors are not the only receptors affecting Ca^{2+} influx and adipogenesis. For example, selective calcium release-activated Ca^{2+} (CRAC) channels prevent the adipocyte differentiation of cells of the 3T3-L1 cell line¹⁶⁶. In addition, transient receptor potential channels and non-selective Ca^{2+} permeation channels also impair adipogenesis by an increased calcium influx¹⁶⁷. Possibly, AMPA-controlled Ca^{2+} influx may intersect with these pathways to influence adipocyte differentiation. Thus, the larger regulatory pathway comprising ADAR2-mediated editing of GRIA2 during adipocyte differentiation remains to be further investigated.

Despite a larger scope of biological experiments and in-depth experimental procedures, this thesis implicates some limitations. 1) Although the initial screening results that formed the basis of this thesis were derived from well-curated patient samples, the experiments of this study were solely performed under *in vitro* conditions in one cell line. In the next step, key findings would need to be confirmed

in a second cell line or primary cells and then verified in an appropriate *in vivo* animal model. 2) The approach of siRNA-mediated gene silencing is technically limited since only a partial inhibition can be accomplished. This implies that residual expression might still have some effects. Full deletion systems could be used to further confirm the main findings. 3) Mechanistically, the study is limited by only investigating one potential ADAR2-dependent gene editing event on GRIA2. To complement the mechanistic landscape, unbiased screens would need to be conducted to obtain further mechanistic insights on how ADRA2 affects adipocyte differentiation.

In summary, this study reports a novel post-transcriptional modification that is mediated by ADAR2 and facilitates the adipocyte differentiation of MSCs. The potential mechanism is that ADAR2 inhibits Ca^{2+} influx by performing A-to-I editing on GRIA2, which promotes adipogenesis by increasing PPAR γ transcriptional activity.

References

1. Clarke, B. Normal Bone Anatomy and Physiology. *Clin. J. Am. Soc. Nephrol.* **3**, S131 (2008).
2. Oreffo, R. O. C., Cooper, C., Mason, C. & Clements, M. Mesenchymal stem cells lineage, plasticity, and skeletal therapeutic potential. *Stem Cell Rev.* **1**, 169–178 (2005).
3. Blair, H. C. *et al.* Osteoblast differentiation and bone matrix formation in vivo and in vitro. *Tissue Engineering - Part B: Reviews* vol. 23 268–280 (2017).
4. Horowitz, M. C. *et al.* Bone marrow adipocytes. *Adipocyte* **6**, 193 (2017).
5. Eyal, S., Rubin, S., Krief, S., Levin, L. & Zelzer, E. Common cellular origin and diverging developmental programs for different sesamoid bones. *Development* **146**, (2019).
6. DiGirolamo, D. J., Clemens, T. L. & Kousteni, S. The skeleton as an endocrine organ. *Nat. Rev. Rheumatol.* **8**, 674–683 (2012).
7. Boskey, A. L. & Robey, P. G. The Composition of Bone. *Prim. Metab. Bone Dis. Disord. Miner. Metab. Eighth Ed.* 49–58 (2013) doi:10.1002/9781118453926.CH6.
8. Allen, M. R., Hock, J. M. & Burr, D. B. Periosteum: biology, regulation, and response to osteoporosis therapies. *Bone* **35**, 1003–1012 (2004).
9. Ascenzi, M. G. & Roe, A. K. The osteon: The micromechanical unit of compact bone. *Front. Biosci.* **17**, 1551–1581 (2012).
10. Singh, I. The architecture of cancellous bone. *J. Anat.* **127**, 305 (1978).
11. E, S. Bone modeling and remodeling. *Crit. Rev. Eukaryot. Gene Expr.* **19**, 219–233 (2009).
12. Teitelbaum, S. L. Bone Resorption by Osteoclasts. *Science (80-.)*. **289**, 1504–1508 (2000).
13. Marks, S. C. & Popoff, S. N. Bone cell biology: The regulation of development, structure, and function in the skeleton. *Am. J. Anat.* **183**, 1–44 (1988).
14. Florencio-Silva, R., Sasso, G. R. da S., Sasso-Cerri, E., Simões, M. J. & Cerri,

- P. S. Biology of Bone Tissue: Structure, Function, and Factors That Influence Bone Cells. *Biomed Res. Int.* **2015**, (2015).
15. C, H., G, G., C, C., O, L. & G, F. EANM Dosimetry Committee guidelines for bone marrow and whole-body dosimetry. *Eur. J. Nucl. Med. Mol. Imaging* **37**, 1238–1250 (2010).
 16. Seita, J. & Weissman, I. L. Hematopoietic stem cell: self-renewal versus differentiation. *Wiley Interdiscip. Rev. Syst. Biol. Med.* **2**, 640–653 (2010).
 17. Birbrair, A., Frenette, P. S. & Biology, C. Niche heterogeneity in the bone marrow. *Ann N Y Acad Sci.* **1370**, 82–96 (2017).
 18. Gurevitch, O., Slavin, S. & Feldman, A. G. Conversion of red bone marrow into yellow – Cause and mechanisms. *Med. Hypotheses* **69**, 531–536 (2007).
 19. Compston, J. E. Bone marrow and bone: A functional unit. *J. Endocrinol.* **173**, 387–394 (2002).
 20. Griffith, J. F. Age-Related Changes in the Bone Marrow. *Curr. Radiol. Rep.* **5**, 1–10 (2017).
 21. Thomas B. Bone Marrow Reconversion in Adults Who Are Smokers: MR Imaging Findings. *AJR* **161**, 1217–1221 (1993).
 22. Friedenstein, A. J., Chailaakhyan, R. K., Latsinik, N. V., Panasyuk, A. F. & Keiliss-Borok, I. V. Stromal cells responsible for transferring the microenvironment of the hemopoietic tissues: Cloning in vitro and retransplantation in vivo. *Transplantation* **17**, 331–340 (1974).
 23. Friedenstein, A. J., Gorskaja, U. F. & Kulagina, N. N. Fibroblast precursors in normal and irradiated mouse hematopoietic organs. *Exp. Hematol.* **4**, 267–274 (1976).
 24. Friedenstein, A. J. *et al.* Precursors for fibroblasts in different populations of hematopoietic cells as detected by the in vitro colony assay method. *Exp. Hematol.* **2**, 83–92 (1974).
 25. Caplan, A. I. Mesenchymal stem cells. *J. Orthop. Res.* **9**, 641–650 (1991).
 26. Dominici, M. *et al.* Minimal criteria for defining multipotent mesenchymal stromal cells. The International Society for Cellular Therapy position statement. *Cytotherapy* **8**, 315–317 (2006).

27. Kemp, K. C., Hows, J. & Donaldson, D. C. Bone marrow-derived mesenchymal stem cells. <https://doi-org.emedien.ub.uni-muenchen.de/10.1080/10428190500215076> **46**, 1531–1544 (2009).
28. Katz, A. J. *et al.* Cell Surface and Transcriptional Characterization of Human Adipose-Derived Adherent Stromal (hADAS) Cells. *Stem Cells* **23**, 412–423 (2005).
29. Kassis, I. *et al.* Isolation of mesenchymal stem cells from G-CSF-mobilized human peripheral blood using fibrin microbeads. *Bone Marrow Transplant.* **37**, 967–976 (2006).
30. Agha-Hosseini, F., Jahani, M. A., Jahani, M., Mirzaii-Dizgah, I. & Ali-Moghaddam, K. In vitro isolation of stem cells derived from human dental pulp. *Clin. Transplant.* **24**, (2010).
31. Meng, X. *et al.* Endometrial regenerative cells: A novel stem cell population. *J. Transl. Med.* **5**, 1–10 (2007).
32. Wouters, G. *et al.* Isolation of amniotic fluid-derived mesenchymal stem cells. *J. Prenat. Med.* **1**, 39 (2007).
33. Pelekanos, R. A. *et al.* Isolation and Expansion of Mesenchymal Stem/Stromal Cells Derived from Human Placenta Tissue. *J. Vis. Exp.* **2016**, 54204 (2016).
34. Zhang, X. *et al.* Isolation and characterization of mesenchymal stem cells from human umbilical cord blood: reevaluation of critical factors for successful isolation and high ability to proliferate and differentiate to chondrocytes as compared to mesenchymal stem cells from bone marrow and adipose tissue. *J. Cell. Biochem.* **112**, 1206–1218 (2011).
35. Pelekanos, R., Venter, D. J. & Australia, S. Comparison of Human Placenta- and Bone Marrow-Derived Multipotent Mesenchymal Stem Cells Article in Stem Cells and Development . (2008) doi:10.1089/scd.2007.0154.
36. Heo, J. S., Choi, Y., Kim, H. S. & Kim, H. O. Comparison of molecular profiles of human mesenchymal stem cells derived from bone marrow, umbilical cord blood, placenta and adipose tissue. *Int. J. Mol. Med.* **37**, 115 (2016).
37. Phinney, D. G. *et al.* Donor variation in the growth properties and osteogenic potential of human marrow stromal cells. *J. Cell. Biochem.* **75**, 424–436 (1999).

38. Zhou, S. *et al.* Age-Related Intrinsic Changes in Human Bone Marrow-Derived Mesenchymal Stem Cells and Their Differentiation to Osteoblasts. *Aging Cell* **7**, 335 (2008).
39. Lee, K. Der *et al.* In vitro hepatic differentiation of human mesenchymal stem cells. *Hepatology* **40**, 1275–1284 (2004).
40. Petersen, B. E. *et al.* Bone marrow as a potential source of hepatic oval cells. *Science* **284**, 1168–1170 (1999).
41. Anghileri, E. *et al.* Neuronal differentiation potential of human adipose-derived mesenchymal stem cells. *Stem Cells Dev.* **17**, 909–916 (2008).
42. Prockop, D. J. & Oh, J. Y. Medical therapies with adult stem/progenitor cells (MSCs): a backward journey from dramatic results in vivo to the cellular and molecular explanations. *J. Cell. Biochem.* **113**, 1460–1469 (2012).
43. Gnocchi, M., Danieli, P., Malpasso, G. & Ciuffreda, M. C. Paracrine Mechanisms of Mesenchymal Stem Cells in Tissue Repair. *Methods Mol. Biol.* **1416**, 123–146 (2016).
44. Gao, F. *et al.* Mesenchymal stem cells and immunomodulation: current status and future prospects. *Cell Death Dis.* **7**, e2062 (2016).
45. Hojo, H., Ohba, S. & Chung, U. II. Signaling pathways regulating the specification and differentiation of the osteoblast lineage. *Regen. Ther.* **1**, 57–62 (2015).
46. Lee, K.-S. *et al.* Runx2 Is a Common Target of Transforming Growth Factor β 1 and Bone Morphogenetic Protein 2, and Cooperation between Runx2 and Smad5 Induces Osteoblast-Specific Gene Expression in the Pluripotent Mesenchymal Precursor Cell Line C2C12. *Mol. Cell. Biol.* **20**, 8783–8792 (2000).
47. Schroeder, T. M., Jensen, E. D. & Westendorf, J. J. Runx2: A master organizer of gene transcription in developing and maturing osteoblasts. *Birth Defects Res. Part C Embryo Today Rev.* **75**, 213–225 (2005).
48. Otto, F., Kanegane, H. & Mundlos, S. Mutations in the RUNX2 gene in patients with cleidocranial dysplasia. *Hum. Mutat.* **19**, 209–216 (2002).
49. Komori, T. *et al.* Targeted disruption of Cbfa1 results in a complete lack of bone

- formation owing to maturational arrest of osteoblasts. *Cell* **89**, 755–764 (1997).
50. Geoffroy, V., Kneissel, M., Fournier, B., Boyde, A. & Matthias, P. High Bone Resorption in Adult Aging Transgenic Mice Overexpressing Cbfa1/Runx2 in Cells of the Osteoblastic Lineage. *Mol. Cell. Biol.* **22**, 6222 (2002).
 51. Liu, W. *et al.* Overexpression of Cbfa1 in osteoblasts inhibits osteoblast maturation and causes osteopenia with multiple fractures. *J. Cell Biol.* **155**, 157–166 (2001).
 52. Ducy, P. & Karsenty, G. R. Two Distinct Osteoblast-Specific cis-Acting Elements Control Expression of a Mouse Osteocalcin Gene. *Mol. Cell. Biol.* **15**, 1858–1869 (1995).
 53. Bruderer, M., Richards, R. G., Alini, M. & Stoddart, M. J. Role and regulation of runx2 in osteogenesis. *Eur. Cells Mater.* **28**, 269–286 (2014).
 54. Yu, S. *et al.* ATF4 Promotes β -Catenin Expression and Osteoblastic Differentiation of Bone Marrow Mesenchymal Stem Cells. *Int. J. Biol. Sci.* **9**, 256 (2013).
 55. K, N. *et al.* The novel zinc finger-containing transcription factor osterix is required for osteoblast differentiation and bone formation. *Cell* **108**, 17–29 (2002).
 56. Li, J., Zhang, H., Yang, C., Li, Y. & Dai, Z. An overview of osteocalcin progress. *J. Bone Miner. Metab.* **34**, 367–379 (2016).
 57. Price, P. A., Otsuka, A. A., Poser, J. W., Kristaponis, J. & Raman, N. Characterization of a gamma-carboxyglutamic acid-containing protein from bone. *Proc. Natl. Acad. Sci.* **73**, 1447–1451 (1976).
 58. Malashkevich, V. N., Almo, S. C. & Dowd, T. L. X-ray crystal structure of bovine 3 Glu-osteocalcin. *Biochemistry* **52**, 8387–8392 (2013).
 59. Ducy, P. *et al.* Increased bone formation in osteocalcin-deficient mice. *Nature* **382**, 448–452 (1996).
 60. Moser, S. C. & van der Eerden, B. C. J. Osteocalcin — A versatile bone-derived hormone. *Front. Endocrinol. (Lausanne)*. **10**, 794 (2019).
 61. Manolagas, S. C. & Parfitt, A. M. What old means to bone. *Trends Endocrinol. Metab.* **21**, 369–374 (2010).

62. Tao, J. *et al.* Osteosclerosis owing to notch gain of function is solely Rbpj-dependent. *J. Bone Miner. Res.* **25**, 2175–2183 (2010).
63. Jochum, W. *et al.* Increased bone formation and osteosclerosis in mice overexpressing the transcription factor Fra-1. *Nat. Med.* **6**, 980–984 (2000).
64. Lowe, C. E., O’Rahilly, S. & Rochford, J. J. Adipogenesis at a glance. *J. Cell Sci.* **124**, 2681–2686 (2011).
65. Rosen, E. D. The transcriptional basis of adipocyte development. *Prostaglandins, Leukot. Essent. Fat. Acids* **73**, 31–34 (2005).
66. Rosen, E. D. & MacDougald, O. A. Adipocyte differentiation from the inside out. *Nat. Rev. Mol. Cell Biol.* **2006 712 7**, 885–896 (2006).
67. Barak, Y. *et al.* PPAR γ Is Required for Placental, Cardiac, and Adipose Tissue Development. *Mol. Cell* **4**, 585–595 (1999).
68. Imai, T. *et al.* Peroxisome proliferator-activated receptor γ is required in mature white and brown adipocytes for their survival in the mouse. *Proc. Natl. Acad. Sci.* **101**, 4543–4547 (2004).
69. Fajas, L. *et al.* The organization, promoter analysis, and expression of the human PPAR γ gene. *J. Biol. Chem.* **272**, 18779–18789 (1997).
70. Hernandez-Quiles, M., Broekema, M. F. & Kalkhoven, E. PPAR γ in Metabolism, Immunity, and Cancer: Unified and Diverse Mechanisms of Action. *Front. Endocrinol. (Lausanne)*. **12**, 1–17 (2021).
71. Mueller, E. *et al.* Genetic Analysis of Adipogenesis through Peroxisome Proliferator-activated Receptor γ Isoforms *. *J. Biol. Chem.* **277**, 41925–41930 (2002).
72. Furuhashi, M. & Hotamisligil, G. S. Fatty acid-binding proteins: role in metabolic diseases and potential as drug targets. *Nat. Rev. Drug Discov.* **2008 76 7**, 489–503 (2008).
73. Furuhashi, M., Saitoh, S., Shimamoto, K. & Miura, T. Fatty Acid-Binding Protein 4 (FABP4): Pathophysiological Insights and Potent Clinical Biomarker of Metabolic and Cardiovascular Diseases. *Clin. Med. Insights. Cardiol.* **8**, 23 (2014).
74. Cabré, A. *et al.* Fatty acid binding protein 4 is increased in metabolic syndrome

- and with thiazolidinedione treatment in diabetic patients. *Atherosclerosis* **195**, (2007).
75. Schachtrup, C., Emmler, T., Bleck, B., Sandqvist, A. & Spener, F. Functional analysis of peroxisome-proliferator-responsive element motifs in genes of fatty acid-binding proteins. *Biochem. J.* **382**, 239–245 (2004).
 76. Yamauchi, T. *et al.* The fat-derived hormone adiponectin reverses insulin resistance associated with both lipodystrophy and obesity. *Nat. Med.* **2001 78 7**, 941–946 (2001).
 77. Gao, Y. *et al.* Silencing of ADIPOQ Efficiently Suppresses Preadipocyte Differentiation in Porcine. *Cell. Physiol. Biochem.* **31**, 452–461 (2013).
 78. Seo, J. B. *et al.* Adipocyte determination- and differentiation-dependent factor 1/sterol regulatory element-binding protein 1c regulates mouse adiponectin expression. *J. Biol. Chem.* **279**, 22108–22117 (2004).
 79. W, H. *et al.* Adipose-specific peroxisome proliferator-activated receptor gamma knockout causes insulin resistance in fat and liver but not in muscle. *Proc. Natl. Acad. Sci. U. S. A.* **100**, 15712–15717 (2003).
 80. Harvey, I., Boudreau, A. & Stephens, J. M. Adipose tissue in health and disease. *Open Biol.* **10**, 200291 (2020).
 81. Cao, J. J. Effects of obesity on bone metabolism. *J. Orthop. Surg. Res.* **2011 61 6**, 1–7 (2011).
 82. Muruganandan, S. & Sinal, C. J. The impact of bone marrow adipocytes on osteoblast and osteoclast differentiation. *IUBMB Life* **66**, 147–155 (2014).
 83. Song, F. *et al.* Association of tissue-specific differentially methylated regions (TDMs) with differential gene expression. *Proc. Natl. Acad. Sci. U. S. A.* **102**, 3336 (2005).
 84. Villagra, A. *et al.* Reduced CpG methylation is associated with transcriptional activation of the bone-specific rat osteocalcin gene in osteoblasts. *J. Cell. Biochem.* **85**, 112–122 (2002).
 85. Fujiki, K., Kano, F., Shiota, K. & Murata, M. Expression of the peroxisome proliferator activated receptor γ gene is repressed by DNA methylation in visceral adipose tissue of mouse models of diabetes. *BMC Biol.* **7**, 38 (2009).

86. Peterson, C. L. & Laniel, M. A. Histones and histone modifications. *Curr. Biol.* **14**, 546–551 (2004).
87. Kouzarides, T. Chromatin Modifications and Their Function. *Cell* **128**, 693–705 (2007).
88. Hemming, S. *et al.* EZH2 and KDM6A Act as an Epigenetic Switch to Regulate Mesenchymal Stem Cell Lineage Specification. *Stem Cells* **32**, 802–815 (2014).
89. Ye, L. *et al.* Histone Demethylases KDM4B and KDM6B Promotes Osteogenic Differentiation of Human MSCs. *Cell Stem Cell* **11**, 50–61 (2012).
90. Bentley, D. L. Coupling mRNA processing with transcription in time and space. *Nat. Rev. Genet.* **15**, 163–175 (2014).
91. Gott, J. M. & Emeson, R. B. FUNCTIONS AND MECHANISMS OF RNA EDITING. (2000).
92. Bass, B. L. RNA editing by adenosine deaminases that act on RNA. *Annual Review of Biochemistry* vol. 71 817–846 (2002).
93. Nishikura, K. Functions and Regulation of RNA Editing by ADAR Deaminases. *Annu. Rev. Biochem.* **79**, 321 (2010).
94. Gallo, A., Vukic, D., Michalík, D., O’Connell, M. A. & Keegan, L. P. ADAR RNA editing in human disease; more to it than meets the I. *Hum. Genet.* **2017** 1369 **136**, 1265–1278 (2017).
95. Snyder, E., Chukrallah, L., Seltzer, K., Goodwin, L. & Braun, R. E. ADAD1 and ADAD2, testis-specific adenosine deaminase domain-containing proteins, are required for male fertility. *Sci. Rep.* **10**, (2020).
96. Kawakubo, K. & Samuel, C. E. Human RNA-specific adenosine deaminase (ADAR1) gene specifies transcripts that initiate from a constitutively active alternative promoter. *Gene* **258**, 165–172 (2000).
97. Lykke-Andersen, S., Piñol-Roma, S. & Kjems, J. Alternative splicing of the ADAR1 transcript in a region that functions either as a 5'-UTR or an ORF. *Rna* **13**, 1732–1744 (2007).
98. Patterson, J. B. & Samuel, C. E. Expression and regulation by interferon of a double-stranded-RNA-specific adenosine deaminase from human cells: evidence for two forms of the deaminase. *Mol. Cell. Biol.* **15**, 5376–5388 (1995).

99. Chen, C. X. *et al.* A third member of the RNA-specific adenosine deaminase gene family, ADAR3, contains both single- and double-stranded RNA binding domains. *RNA* **6**, 755–767 (2000).
100. Goodman, R. A., MacBeth, M. R. & Beal, P. A. ADAR proteins: Structure and catalytic mechanism. *Curr. Top. Microbiol. Immunol.* **353**, 1–33 (2012).
101. Cho, D. S. C. *et al.* Requirement of dimerization for RNA editing activity of adenosine deaminases acting on RNA. *J. Biol. Chem.* **278**, 17093–17102 (2003).
102. Chilibeck, K. A. *et al.* FRET analysis of in vivo dimerization by RNA-editing enzymes. *J. Biol. Chem.* **281**, 16530–16535 (2006).
103. Nishikura, K. *et al.* Substrate specificity of the dsRNA unwinding/modifying activity. *EMBO J.* **10**, 3523–3532 (1991).
104. Lehmann, K. A. & Bass, B. L. The importance of internal loops within RNA substrates of ADAR1. *J. Mol. Biol.* **291**, 1–13 (1999).
105. Hocine, S., Singer, R. H. & Grünwald, D. RNA processing and export. *Cold Spring Harb. Perspect. Biol.* **2**, 1–20 (2010).
106. Traynelis, S. F. *et al.* Glutamate receptor ion channels: Structure, regulation, and function. *Pharmacol. Rev.* **62**, 405–496 (2010).
107. Higuchi, M. *et al.* RNA editing of AMPA receptor subunit GluR-B: A base-paired intron-exon structure determines position and efficiency. *Cell* **75**, 1361–1370 (1993).
108. Higuchi, M. *et al.* Point mutation in an AMPA receptor gene rescues lethality in mice deficient in the RNA-editing enzyme ADAR2. *Nature* **406**, 78–81 (2000).
109. Bhakta, S., Azad, M. T. A. & Tsukahara, T. Genetic code restoration by artificial RNA editing of Ochre stop codon with ADAR1 deaminase. *Protein Eng. Des. Sel.* **31**, 471–478 (2018).
110. Bhakta, S. & Tsukahara, T. Double MS2 guided restoration of genetic code in amber (TAG), opal (TGA) and ochre (TAA) stop codon. *Enzyme Microb. Technol.* **149**, 109851 (2021).
111. Cook, G. W. *et al.* A Comparison of 100 Human Genes Using an Alu Element-Based Instability Model. *PLoS One* **8**, (2013).

112. Licht, K. *et al.* A high resolution A-to-I editing map in the mouse identifies editing events controlled by pre-mRNA splicing. *Genome Res.* **29**, 1453–1463 (2019).
113. Athanasiadis, A., Rich, A. & Maas, S. Widespread A-to-I RNA editing of Alu-containing mRNAs in the human transcriptome. *PLoS Biol.* **2**, (2004).
114. Blow, M., Futreal, A. P., Wooster, R. & Stratton, M. R. A survey of RNA editing in human brain. *Genome Res.* **14**, 2379–2387 (2004).
115. Kim, D. D. Y. *et al.* Widespread RNA editing of embedded Alu elements in the human transcriptome. *Genome Res.* **14**, 1719–1725 (2004).
116. Levanon, E. Y. *et al.* Systematic identification of abundant A-to-I editing sites in the human transcriptome. *Nat. Biotechnol.* **22**, 1001–1005 (2004).
117. Valente, L. & Nishikura, K. ADAR Gene Family and A-to-I RNA Editing: Diverse Roles in Posttranscriptional Gene Regulation. *Prog. Nucleic Acid Res. Mol. Biol.* **79**, 299–338 (2005).
118. Rueter, S. M., Dawson, T. R. & Emeson, R. B. Regulation of alternative splicing by RNA editing. *Nature* **399**, 75–80 (1999).
119. Prasanth, K. V. *et al.* Regulating gene expression through RNA nuclear retention. *Cell* **123**, 249–263 (2005).
120. Bass, B. L. Double-stranded RNA as a template for gene silencing. *Cell* vol. 101 235–238 (2000).
121. Borchert, G. M. *et al.* Adenosine deamination in human transcripts generates novel microRNA binding sites. *Hum. Mol. Genet.* **18**, 4801–4807 (2009).
122. Livingston, J. H. *et al.* A type I interferon signature identifies bilateral striatal necrosis due to mutations in ADAR1. *J. Med. Genet.* **51**, 76–82 (2014).
123. M, H. & T, S. A missense mutation c.G2747A (p.R916Q) of ADAR1 gene in dyschromatosis symmetrica hereditaria is not a novel mutation. *Arch. Dermatol. Res.* **302**, 481–482 (2010).
124. Tan, T. Y. *et al.* Bi-allelic ADARB1 Variants Associated with Microcephaly, Intellectual Disability, and Seizures. *Am. J. Hum. Genet.* **106**, 467–483 (2020).
125. Chen, L. *et al.* Recoding RNA editing of AZIN1 predisposes to hepatocellular

- carcinoma. *Nat. Med.* 2013 192 **19**, 209–216 (2013).
126. Fumagalli, D. *et al.* Principles Governing A-to-I RNA Editing in the Breast Cancer Transcriptome. *Cell Rep.* **13**, 277–289 (2015).
 127. Jiang, Q. *et al.* ADAR1 promotes malignant progenitor reprogramming in chronic myeloid leukemia. *Proc. Natl. Acad. Sci.* **110**, 1041–1046 (2013).
 128. Galeano, F. *et al.* ADAR2-editing activity inhibits glioblastoma growth through the modulation of the CDC14B/Skp2/p21/p27 axis. *Oncogene* 2013 328 **32**, 998–1009 (2012).
 129. Simonsen, J. L. *et al.* Telomerase expression extends the proliferative life-span and maintains the osteogenic potential of human bone marrow stromal cells. *Nat. Biotechnol.* **20**, 592–596 (2002).
 130. Rauch, A. *et al.* Osteogenesis depends on commissioning of a network of stem cell transcription factors that act as repressors of adipogenesis. doi:10.1038/s41588-019-0359-1.
 131. Goodpaster, B. H., Kelley, D. E., Thaete, F. L., He, J. & Ross, R. Skeletal muscle attenuation determined by computed tomography is associated with skeletal muscle lipid content. *J. Appl. Physiol.* **89**, 104–110 (2000).
 132. Lehmann, K. A. & Bass, B. L. Double-Stranded RNA Adenosine Deaminases ADAR1 and ADAR2 Have Overlapping Specificities †. (2000) doi:10.1021/bi001383g.
 133. Seeburg, P. H. & Hartner, J. Regulation of ion channel/neurotransmitter receptor function by RNA editing. *Current Opinion in Neurobiology* vol. 13 279–283 (2003).
 134. Teven, C. M. *et al.* Epigenetic regulation of mesenchymal stem cells: A focus on osteogenic and adipogenic differentiation. *Stem Cells Int.* **2011**, (2011).
 135. Augello, A. & De Bari, C. The Regulation of Differentiation in Mesenchymal Stem Cells. <https://home.liebertpub.com/hum> **21**, 1226–1238 (2010).
 136. Lefterova, M. I., Haakonsson, A. K., Lazar, M. A. & Mandrup, S. PPAR γ and the global map of adipogenesis and beyond. *Trends Endocrinol. Metab.* **25**, 293–302 (2014).
 137. Peng, P. L. *et al.* ADAR2-dependent RNA editing of AMPA receptor subunit

- GluR2 determines vulnerability of neurons in forebrain ischemia. *Neuron* **49**, 719–733 (2006).
138. Zhang, R. *et al.* Transcriptional Regulation of BMP2 Expression by the PTH-CREB Signaling Pathway in Osteoblasts. *PLoS One* **6**, e20780 (2011).
139. Zhang, J. W., Klemm, D. J., Vinson, C. & Lane, M. D. Role of CREB in Transcriptional Regulation of CCAAT/Enhancer-binding Protein β Gene during Adipogenesis *. *J. Biol. Chem.* **279**, 4471–4478 (2004).
140. Yu, S. *et al.* ADAR1 ablation decreases bone mass by impairing osteoblast function in mice. *Gene* **513**, 101 (2013).
141. Riedmann, E. M., Schopoff, S., Hartner, J. C. & Jantsch, M. F. Specificity of ADAR-mediated RNA editing in newly identified targets. *Rna* **14**, 1110–1118 (2008).
142. Galipon, J., Ishii, R., Suzuki, Y., Tomita, M. & Ui-Tei, K. Differential binding of three major human ADAR isoforms to coding and long non-coding transcripts. *Genes (Basel)*. **8**, 1–13 (2017).
143. Singh, M. *et al.* Hyperphagia-mediated Obesity in Transgenic Mice Misexpressing the RNA-editing Enzyme ADAR2 *. *J. Biol. Chem.* **282**, 22448–22459 (2007).
144. Akubuiro, A. *et al.* Hyperactive hypothalamus, motivated and non-distractible chronic overeating in ADAR2 transgenic mice. *Genes, Brain Behav.* **12**, 311–322 (2013).
145. Singh, M., Zimmerman, M. B., Beltz, T. G. & Johnson, A. K. Affect-related behaviors in mice misexpressing the RNA editing enzyme ADAR2. *Physiol. Behav.* **97**, 446–454 (2009).
146. Gan, Z. *et al.* RNA Editing by ADAR2 Is Metabolically Regulated in Pancreatic Islets and β -Cells *. *J. Biol. Chem.* **281**, 33386–33394 (2006).
147. L, Y. *et al.* Deficiency in RNA editing enzyme ADAR2 impairs regulated exocytosis. *FASEB J.* **24**, 3720–3732 (2010).
148. Farmer, S. R. Transcriptional control of adipocyte formation. *Cell Metab.* **4**, 263–273 (2006).
149. Lefterova, M. I. *et al.* PPAR γ and C/EBP factors orchestrate adipocyte biology

- via adjacent binding on a genome-wide scale. *Genes Dev.* **22**, 2941–2952 (2008).
150. Tontonoz, P., Hu, E. & Spiegelman, B. M. Stimulation of adipogenesis in fibroblasts by PPAR γ 2, a lipid-activated transcription factor. *Cell* **79**, 1147–1156 (1994).
 151. Rosen, E. D. *et al.* C/EBP α induces adipogenesis through PPAR γ : a unified pathway. *Genes Dev.* **16**, 22 (2002).
 152. Wu, Z. *et al.* Cross-regulation of C/EBP alpha and PPAR gamma controls the transcriptional pathway of adipogenesis and insulin sensitivity. *Mol. Cell* **3**, 151–158 (1999).
 153. Hu, E., Kim, J. B., Sarraf, P. & Spiegelman, B. M. Inhibition of Adipogenesis Through MAP Kinase-Mediated Phosphorylation of PPAR γ . *Science (80-.)*. **274**, 2100–2103 (1996).
 154. Zhang, B. *et al.* Insulin- and Mitogen-activated Protein Kinase-mediated Phosphorylation and Activation of Peroxisome Proliferator-activated Receptor γ *. *J. Biol. Chem.* **271**, 31771–31774 (1996).
 155. Choi, J. H. *et al.* Anti-diabetic drugs inhibit obesity-linked phosphorylation of PPAR γ by Cdk5. *Nat. 2010 4667305* **466**, 451–456 (2010).
 156. Floyd, Z. E. & Stephens, J. M. Control of Peroxisome Proliferator-Activated Receptor γ 2 Stability and Activity by SUMOylation. *Obes. Res.* **12**, 921–928 (2004).
 157. Horsch, M. *et al.* Requirement of the RNA-editing Enzyme ADAR2 for Normal Physiology in Mice *. *J. Biol. Chem.* **286**, 18614–18622 (2011).
 158. Nicolaysen, A., Gammelsaeter, R., Storm-Mathisen, J., Gundersen, V. & Iversen, P. O. The components required for amino acid neurotransmitter signaling are present in adipose tissues. *J. Lipid Res.* **48**, 2123–2132 (2007).
 159. Ikegami, R. *et al.* Gamma-Aminobutyric Acid Signaling in Brown Adipose Tissue Promotes Systemic Metabolic Derangement in Obesity. *Cell Rep.* **24**, 2827-2837.e5 (2018).
 160. Takahashi, A., Camacho, P., Lechleiter, J. D. & Herman, B. Measurement of intracellular calcium. *Physiol. Rev.* **79**, 1089–1125 (1999).

161. Clapham, D. E. Calcium Signaling. *Cell* **131**, 1047–1058 (2007).
162. Goudarzi, F. *et al.* The Role of Calcium in Differentiation of Human Adipose-Derived Stem Cells to Adipocytes. *Mol. Biotechnol.* **60**, 279–289 (2018).
163. Pramme-Steinwachs, I., Jastroch, M. & Ussar, S. Extracellular calcium modulates brown adipocyte differentiation and identity. *Sci. Rep.* **7**, 1–10 (2017).
164. Ntambi, J. M. & Takova, T. Role of Ca²⁺ in the early stages of murine adipocyte differentiation as evidenced by calcium mobilizing agents. *Differentiation* **60**, 151–158 (1996).
165. SHI, H., HALVORSEN, Y.-D., ELLIS, P. N., WILKISON, W. O. & ZEMEL, M. B. Role of intracellular calcium in human adipocyte differentiation. <https://doi.org/10.1152/physiolgenomics.2000.3.2.75> **2000**, 75–82 (2000).
166. Graham, S. J. L. *et al.* Stim1, an endoplasmic reticulum Ca²⁺ sensor, negatively regulates 3T3-L1 pre-adipocyte differentiation. *Differentiation* **77**, 239–247 (2009).
167. Zhang, L. L. *et al.* Activation of Transient Receptor Potential Vanilloid Type-1 Channel Prevents Adipogenesis and Obesity. *Circ. Res.* **100**, 1063–1070 (2007).

Acknowledgements

I started this thesis in the Molecular Skeletal Biology Laboratory at the University Medical Center Hamburg-Eppendorf in Hamburg, Germany in October 2018. During the time of my thesis, my supervisor Prof. Dr. Eric Hesse assumed the position as chair of the newly founded Institute of Musculoskeletal Medicine at the Hospital of the Ludwig-Maximilians-University in Munich, Germany and I therefore continued and finished my project there starting in January 2020. During my time in the laboratory, I received plenty of support. Here I would like to express my gratitude to all people who helped me with this study.

First, I would like to express my deepest gratitude to my supervisor Prof. Dr. Eric Hesse. Thank you for providing this great opportunity. It is my pleasure that I had the chance to conduct my research under your supervision. Without your support and academic guidance, this study would not have been accomplished. I would also like to say thank you to my co-supervisor Prof. Dr. Hanna Taipaleenmäki. Thank you for giving me so much advice on my research project and for providing great help with my thesis. Your support and guidance helped me a lot. I would also like to thank PD. Dr. Attila Aszódi for critical review of my project and thesis and for providing helpful input. I also thank you for providing a temporary lab environment when I arrived in Munich.

I would like to thank Dr. Hiroaki Saito. Thank you for teaching me so many research skills as well as for providing technical help. In addition, I thank Ramona Mettler, Jennifer Zarrer, Chiara di Scullo, and all previous and current lab members for their great support and company. It has been a great experience to work together with you. I feel very lucky being your teammate.

A great thank you is also dedicated to my friends in Germany. Your support in daily life and companionship made my experience abroad quite colorful.

Finally, I would like to thank my family, especially my parents, my parents-in-law, my wife, and my two-year-old daughter. Your encouragements and supports are the endless source of my motivation.

Affidavit



Eidesstattliche Versicherung

Tang, Rui

Name, Vorname

Ich erkläre hiermit an Eides statt, dass ich die vorliegende Dissertation mit dem Titel:

Investigating the role of ADAR2 in osteoblast and adipocyte differentiation

selbständig verfasst, mich außer der angegebenen keiner weiteren Hilfsmittel bedient und alle Erkenntnisse, die aus dem Schrifttum ganz oder annähernd übernommen sind, als solche kenntlich gemacht und nach ihrer Herkunft unter Bezeichnung der Fundstelle einzeln nachgewiesen habe.

Ich erkläre des Weiteren, dass die hier vorgelegte Dissertation nicht in gleicher oder in ähnlicher Form bei einer anderen Stelle zur Erlangung eines akademischen Grades eingereicht wurde.

München, 17.11.2022

Ort, Datum

Rui Tang

Unterschrift Doktorandin bzw. Doktorand